

Liquid chromatography with dual parallel mass spectrometry and ^{31}P nuclear magnetic resonance spectroscopy for analysis of sphingomyelin and dihydrosphingomyelin II. Bovine milk sphingolipids

Wm. Craig Byrdwell^{a,*}, Richard H. Perry^b

^a USDA, ARS, BHNRC, FCL, Beltsville, MD 20904, USA

^b Department of Chemistry, Purdue University, West Lafayette, IN 47907, USA

Received 24 October 2006; received in revised form 25 January 2007; accepted 29 January 2007

Available online 3 February 2007

Abstract

Liquid chromatography coupled to atmospheric pressure chemical ionization (APCI) and electrospray ionization (ESI) mass spectrometry (MS), in parallel, was used for simultaneous detection of bovine milk sphingolipids (BMS). APCI-MS mass spectra exhibited mostly ceramide-like fragment ions, $[\text{Cer-H}_2\text{O} + \text{H}]^+$ and $[\text{Cer-2H}_2\text{O} + \text{H}]^+$, which were used to identify individual molecular species of BMS according to fatty acyl chain length: degree of unsaturation and long-chain base (LCB). ESI-MS was used to confirm the molecular weights of BMS species. Both sphingomyelin (SM) and dihydrosphingomyelin (DSM) molecular species were identified, with DSM species constituting 20% of BMS. Approximately 56 to 58% of DSM species contained a *d*16:0 LCB, while 34 to 37% contained a *d*18:0 LCB. Approximately 26 to 30% of SM species contained a *d*16:1 LCB, while 57 to 60% contained a *d*18:1 LCB. BMS species contained both odd and even carbon chain lengths. The most abundant DSM species contained a *d*16:0 LCB with a 22:0, 23:0 or 24:0 fatty acyl chain, while the most abundant SM species contained a *d*18:1 LCB with a 16:0 or 23:0 fatty acyl chain. ^{31}P NMR spectroscopy was used to conclusively confirm that DSM is a dietary component in BMS. Crown Copyright © 2007 Published by Elsevier B.V. All rights reserved.

Keywords: Sphingomyelin; Dihydrosphingomyelin; Sphingolipids; Phospholipids; Mass spectrometry; APCI-MS; ESI-MS; Atmospheric pressure chemical ionization; Electrospray ionization

1. Introduction

It has been well demonstrated that sphingomyelin (SM) acts as the substrate for *sphingomyelinase*, to produce the potent cell signaling molecule ceramide, in a process referred to as the Sphingomyelin Cycle [1–3]. Ceramide, the product of the Sphingomyelin Cycle, has been implicated in initiating cellular signaling processes from apoptosis to lipid transport to ion channel operation and many others, as evidenced by numerous studies using synthetic ceramide [4–13]. A few studies have also been done on dihydroceramide that demonstrated that it

is often much less active in the same signaling pathways in which ceramide is so active [14–17]. The lack of the 4,5 *trans* double bond in dihydroceramide may give it the opposite behavior from its closely related structural analog ceramide in many cellular systems. However, this general rule is not universally true [18].

Studies have shown that the *sphingomyelinase* acts on dihydrosphingomyelin (DSM) just as efficiently (perhaps even more so) as it does on SM [19]. Thus, dihydroceramide, the often inactive signaling molecule, is produced with equal efficiency as ceramide, the active signaling molecule, by treatment of sphingolipids (SLs), which may contain SM or DSM, with *sphingomyelinase*. This sets up the potential for a competitive activation/inhibition system, in which the relative amounts of DSM and SM determine the amount of activation of cellular systems by action of *sphingomyelinase* on a mixture of SLs to produce either ceramide or dihydroceramide. Thus, it is impor-

* Corresponding author at: Food Composition Laboratory, USDA, ARS, BHNRC, Beltsville, MD 20705, USA. Tel.: +1 301 504 9357; fax: +1 301 504 8314.

E-mail address: Byrdwell@ba.ars.usda.gov (Wm.C. Byrdwell).

URL: <http://www.byrdwell.com> (Wm.C. Byrdwell).

tant to know the relative amounts of these two classes in a mixture of SLs.

Some work has been done on phytoceramides, a type of hydroxyceramides, that indicates that they are even more active in cellular signaling processes than normal ceramide [20], although it must be realized that the hydroxy group in phytoceramide is on the long-chain base (LCB), instead of on the fatty acid (FA) chain. [Note that it is common practice to refer to the amide-linked hydrocarbon chain as a fatty acid, even though to be technically accurate, it is a fatty amide.] Thus, if hydroxy-containing SLs were present, which would lead to formation of hydroxyceramide, more activation of cellular activity might be expected from the products of *sphingomyelinase* hydrolysis on these molecules than from normal ceramide. If hydroxyceramide having the hydroxyl group on the FA behaves at all similarly to phytoceramide, it might also show enhanced activity. On the other hand, if a substantial proportion of DSM species are identified, this might lead to the expectation for less activation of cellular activity, due to the potential for competitive activation/inhibition between ceramide and dihydroceramide. Thus, proper identification of the molecular species of dihydrosphingomyelin species, and distinguishing them from species containing hydroxyl moieties, could be an important prerequisite for proper understanding of the effects of SLs on cellular activity.

Since phosphosphingolipids are large (~700–900 Da) zwitterionic molecules, they are not amenable to direct gas-phase analysis using techniques such as gas chromatography (GC) or GC/MS. In the past, sphingomyelin species were typically derivatized to produce methyl esters from the fatty amide chain [21]. Other derivatives, such as dinitrophenyl [22] or trimethylsilyl (TMS) ethers [23,24], were used for analysis of the LCB. TMS derivatives of ceramides have also been reported [25]. Bovine milk sphingolipids (BMS) have been analyzed and reports on these were recently reviewed [26]. Older MS applications for sphingolipid analysis were reviewed in 1993 [27]. Although effective, methods based on derivatization are labor-intensive and time-consuming.

In a recent report [28], we demonstrated the use of a ‘dual parallel mass spectrometer’ arrangement for identification of the molecular species of sphingomyelin and dihydrosphingomyelin from bovine brain and chicken egg sphingolipid samples. In contrast to most previous literature reports that used LC/MS, we reported a substantial proportion of dihydrosphingomyelin species in bovine brain, in addition to the commonly reported sphingomyelin species. The significant proportion of DSM species was confirmed by ^{31}P NMR spectroscopy, and agreed well with our previous results [29] and results by older derivatization methods [21], which had showed a substantial contribution from DSM species.

In the preceding report [28], we demonstrated that APCI-MS of SLs produced ceramide-like fragment ions and showed that MS/MS could be used to identify the LCB portion of a SL molecule, while fragments derived from the fatty amide chain identified its carbon chain length and degree of unsaturation. The ceramide-like fragments were the same as those formed by

APCI-MS of ceramide [30], and were equivalent to a protonated ceramide molecule minus a mole of water, $[\text{Cer-H}_2\text{O} + \text{H}]^+$, and also loss of two moles of water, $[\text{Cer-2H}_2\text{O} + \text{H}]^+$. Two fatty acyl chain-related fragments were described as $[\text{FA}(\text{long})]^+$ and $[\text{FA}(\text{short})]^+$. The former contained the fatty amide chain plus two carbons from the serine backbone of the SL, while the latter was formed by cleavage between the nitrogen and the backbone carbon to produce a free amine. The structures of those and other fragments were given in Figs. 4 and 5 in our report [28]. ESI-MS produced protonated molecules, $[\text{M} + \text{H}]^+$, that confirmed the identities of molecular species identified by APCI-MS.

In this report, we demonstrate the use of APCI-MS and ESI-MS in a dual parallel mass spectrometry (MS) arrangement for analysis of BMS. These SLs are more complex than bovine brain or chicken egg SLs. BMS contain a greater diversity of both long-chain bases and fatty amide chains, including odd carbon chain lengths. We highlight the shortcomings and inherent pitfalls of sphingolipid analysis, and demonstrate the importance of using multiple mutually confirmatory techniques to produce the most reliable results. We present ^{31}P NMR spectroscopy data that confirm the results obtained by APCI-MS and ESI-MS and show that DHS is a dietary sphingolipid, constituting approximately 20% of BMS.

2. Experimental

2.1. Materials

All solvents were HPLC quality and were purchased from Sigma Aldrich (Milwaukee, WI, USA) or Fisher Scientific (Fair Lawn, NJ, USA) and were used without further purification. Bovine milk sphingomyelin and dipalmitoyl glycerophosphocholine were purchased from Avanti Polar Lipids (Alabaster, AL, USA). A solution of 10.58 mg/mL of the BMS in chloroform with 0.50 mg/mL of dipalmitoyl glycerophosphocholine added as an internal standard was used for the LC/MS analysis. Three separate samples having an average concentration of 25.6 mg/mL BMS in deuteriochloroform with 10.6 mg/mL dipalmitoyl glycerophosphocholine were prepared for replicate ^{31}P NMR spectroscopy experiments.

2.2. High performance liquid chromatography

The present study employed a normal phase (NP) HPLC method that was optimized specifically for maximum resolution of the classes of sphingomyelin and dihydrosphingomyelin to the exclusion of other phospholipid classes. The NP-HPLC system consisted of an AS3000 autosampler, a TSP4000 quaternary gradient pump with membrane degasser, a UV6000LP diode array detection (DAD) system (Thermo Separation Products, Thermo Electron, San Jose, CA, USA) and a CH-430 column heater (Eppendorf, Westbury, NY) set at 57 °C. Two Adsorbosphere NH_2 columns (Alltech Associates, Deerfield, IL, USA), 25.0 cm \times 4.6 mm, with 5 μm particles, were used in series. These were joined by a piece of 0.01 in. I.D. stain-

less steel tubing with a circular bend such that the columns were parallel in the column heater. The columns were equilibrated for one hour before the first experiment each day, and for 15 min between runs. A model MKIII evaporative light scattering detection (ELSD) system (Varex, Burtonsville, MD, USA) was used as an auxiliary detector, attached to the TSQ700 mass spectrometer. The drift tube was operated at 140 °C, with the UHP N₂ nebulizer gas pressure at 47 psi.

The solvents used were: solvent A, 40% hexane (Hex)/60% isopropanol (IPA) and solvent B, 40% H₂O/60% IPA, both with 0.1% NH₄OH. The gradient program was: from 0 to 50 min, 77% A: 23% B; from 50 to 55 min linear to 50% A: 50% B, held until 75 min; from 75 to 80 min recycled to initial conditions and held until 95 min to equilibrate columns at initial conditions between runs. The flow rate was 0.8 mL/min throughout and the injection volume was 10.0 µL.

2.3. Dual parallel mass spectrometry

The dual parallel mass spectrometer arrangement used for semi-quantitative analysis consisted of APCI-MS performed on the LCQ Deca ion trap mass spectrometry (ITMS) instrument and ESI-MS performed using the TSQ700 triple-stage quadrupole instrument from the same column eluate. In some runs used for qualitative analysis, positive- and negative-ion ESI-MS was performed on the ITMS in parallel with positive-ion APCI-MS on the TSQ700 instrument. Negative-ion APCI-MS, MS/MS and MSⁿ experiments were performed on the ITMS instrument, without parallel runs on the TSQ700. Numerous positive-ion APCI-MSⁿ runs were performed on specific subsets of precursor ions manually identified from full scans, to obtain MS/MS and MS³ data from all molecular species, even those present at low levels. Other combinations of ESI and APCI on either or both mass spectrometers were used, but not reported. The dual parallel mass spectrometers and auxiliary detectors were attached as described in detail elsewhere [28,29].

2.4. Electrospray Ionization mass spectrometry (ESI-MS) and MSⁿ

In dual parallel MS experiments in which ESI-MS was performed on the TSQ700 mass spectrometer, the instrument was operated in Q3 mode, with Q1 set to pass all ions. The heated capillary temperature was 265 °C. The ESI needle voltage was 5.5 kV. The UHP N₂ sheath and auxiliary gases were operated at 35 psi and 5 mL/min, respectively. A solution of 20 mM ammonium formate in H₂O:ACN (1:4), described previously [31], was added directly to the ESI source as a sheath liquid at 20 µL/min, supplied from an AB 140B syringe pump (Applied Biosystems, Foster City, CA). Scans were obtained positive-ion mode in the range *m/z* 150 to 2000 with a scan time of 1.42 s. For ESI-MS experiments on the LCQ Deca ion trap instrument, scans were obtained from *m/z* 200 to 2000, the sheath gas flow was 40 (arbitrary units) and the auxiliary gas flow rate was 5 (arbitrary

units) and all other source parameters were the same as on the TSQ700.

2.5. Atmospheric pressure chemical ionization mass spectrometry (APCI-MS) and MSⁿ

In dual parallel MS experiments with APCI-MS performed on the LCQ Deca ion trap mass spectrometer, the heated capillary temperature was 265 °C, the vaporizer temperature was 475 °C and the corona discharge needle current was 6.0 µA. The sheath gas flow was 40 (arb. units) and the auxiliary gas flow rate was 5 (arb. units). APCI-MS scans were obtained in the range *m/z* 200–1200.

2.6. ³¹P Nuclear magnetic resonance (NMR) spectroscopy

The solution of the commercially available BMS in chloroform was taken to dryness under Argon in a tared vial and reconstituted in deuterated chloroform with a concentration of 25.3 mg/mL, with 10.6 mg/mL of dipalmitoyl glycerophosphocholine added as the internal standard, and to provide calibration of the chemical shift axis. The chemical shift of dipalmitoyl glycerophosphocholine was set to -0.840δ , according to the method of Meneses and Glonek [32]. 800 µL of the sample mixture was transferred to a 5 mm NMR tube and 400 µL of the Meneses–Glonek reagent was added [32]. CsOH was used for the cation to yield the Cs-EDTA complex, and H₂O was used to prepare the solution, since the deuterium lock signal was provided by CDCl₃.

3. Results and discussion

Fig. 1 shows the total ion current chromatogram (TIC) obtained by APCI-MS, and mass spectra averaged across the three sphingolipid peaks. All mass spectra in Fig. 1 showed that the sphingolipids produced two ceramide-related fragment ions, [Cer-H₂O + H]⁺ and [Cer-2H₂O + H]⁺, which provided information about the combined long-chain bases and the fatty amide chains. Fig. 1B, which is an average APCI-MS mass spectrum across SL1, showed the [Cer-H₂O + H]⁺ and [Cer-2H₂O + H]⁺ fragments that corresponded to long-chain DSM species. For DSM species, the [Cer-H₂O + H]⁺ peaks were larger than the [Cer-2H₂O + H]⁺ peaks. The absence of the 4,5 *trans* double bond appeared to make it less favorable for the hydroxy group to leave. The *m/z* 266.4 peak in Fig. 1B arising from the LCBs of the DSM species is smaller, relative to the [Cer-H₂O + H]⁺ peaks, than the *m/z* 264.4 peak in Fig. 1C and D, relative to the [Cer-H₂O + H]⁺ and [Cer-2H₂O + H]⁺ peaks arising from SM species. This trend was similarly observed from bovine brain sphingolipids [28]. The low abundances of the [LCB-H₂O]⁺ fragments from DSM species indicated that the 4,5 *trans* double bond caused a difference in the energy of fragmentation of the LCB fragments of DSM species compared to the SM species. The calculated monoisotopic masses of all fragments, protonated molecules and adducts discussed herein are given at www.sphingomyelin.com.

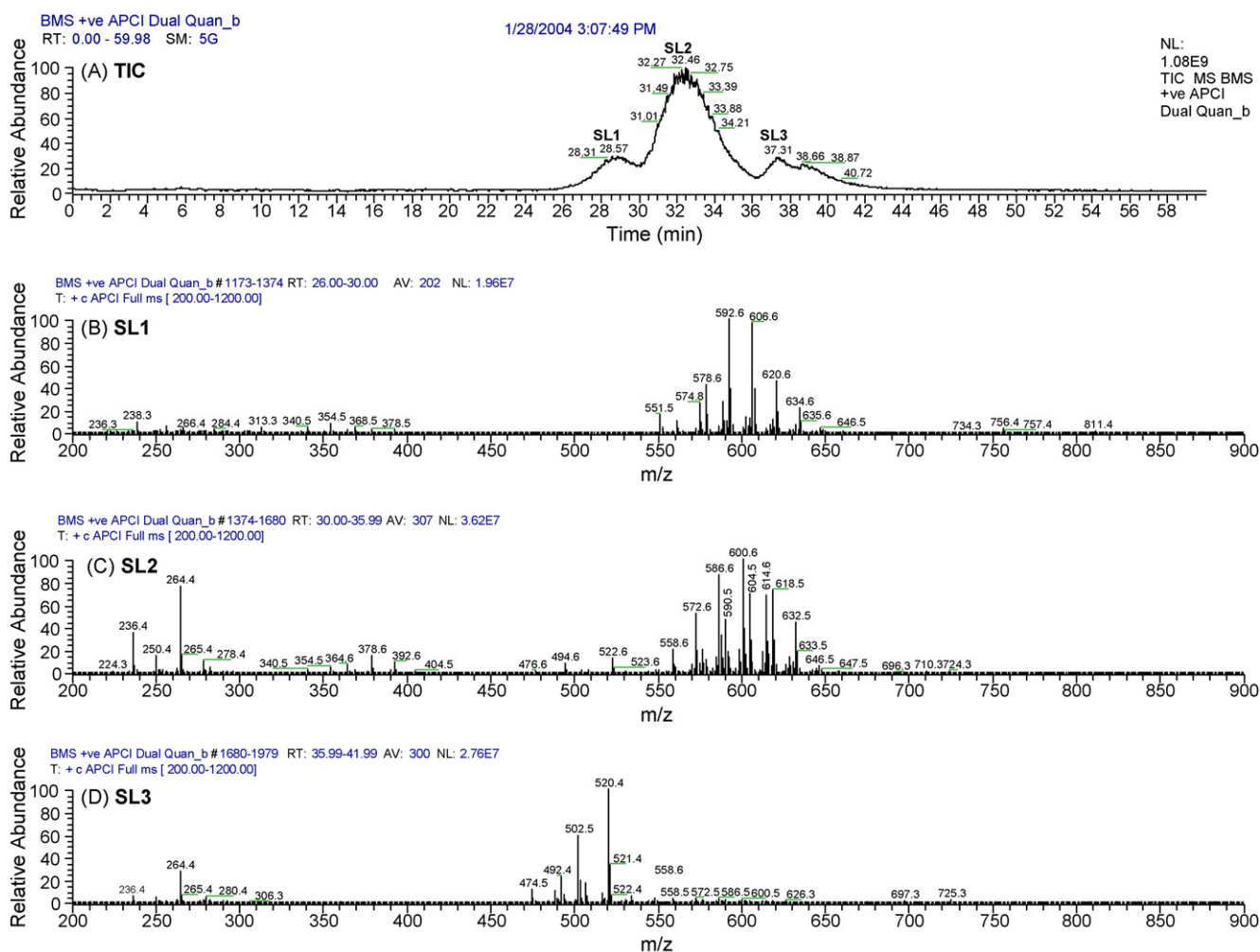


Fig. 1. APCI-MS total ion current chromatogram (TIC) and full-scan mass spectra. (A) TIC; (B) averaged mass spectrum across sphingolipid peak 1, SL1, from 26 to 30 min; (C) averaged mass spectrum across SL2, from 30 to 36 min; (D) averaged mass spectrum across SL3, from 36 to 42 min. Obtained in parallel with run shown in Fig. 2.

3.1. Full-scan APCI-MS mass spectra

The primary $[\text{Cer-H}_2\text{O} + \text{H}]^+$ peaks in Fig. 1B were at m/z 634.6, m/z 620.6, m/z 606.6, m/z 592.6, and m/z 578.6. If these all had 18-carbon long-chain bases, they would correspond to $d18:0/24:0$, $d18:0/23:0$, $d18:0/22:0$, $d18:0/21:0$, and $d18:0/20:0$, respectively. Milk SLs did not all have 18-carbon LCBs, but the masses serve to illustrate several points. First, the species present in the largest amounts in milk SLs had saturated fatty amide chains. Second, there were large quantities of species with odd carbon chains, as well as even. Third, the saturated DSM species were not isobaric with any SM species, so the saturated species were readily identifiable. Species that had monounsaturated fatty amide chains were also apparent, but they had smaller abundances compared to the primary peaks mentioned above. Although it would appear that species having two sites of unsaturation were also present at 4 m/z lower than each of the peaks mentioned above, MS/MS and MS³ data indicated that these ions actually arose from $[\text{Cer-2H}_2\text{O} + \text{H}]^+$ peaks. APCI-MS full-scan mass spectra must be carefully interpreted to avoid misidentification of molecular species. No species containing two or

more sites of unsaturation were identified with sufficient certainty to allow semi-quantification, based on the FA fragments in the MS/MS and MS³ spectra. The MS/MS data allowed the identities of several different saturated long-chain bases that contributed to each group of isobaric species having the masses given above to be determined. A semi-quantitative estimation of the composition of the long-chain bases that made up the group of isobaric DSM species, determined by APCI-MS, MS/MS and MS³, is given in Table 1.

Fig. 1C shows the average mass spectrum across SL2. The $[\text{Cer-H}_2\text{O} + \text{H}]^+$ peaks at m/z 522.6, m/z 504.6, and m/z 494.6 indicated elution of short-chain DSM species in SL2. However, the primary $[\text{Cer-H}_2\text{O} + \text{H}]^+$ peaks produced by SLs eluted in SL2 were at m/z 632.5, m/z 618.5, m/z 604.5, m/z 590.5 and m/z 576.5. These fragment masses indicated elution of long-chain SM species. These peaks gave corresponding $[\text{Cer-2H}_2\text{O} + \text{H}]^+$ peaks at m/z 614.6, m/z 600.6, m/z 586.6, m/z 572.6 and m/z 558.6, respectively. Fig. 1C showed that the $[\text{Cer-2H}_2\text{O} + \text{H}]^+$ peaks were larger than the $[\text{Cer-H}_2\text{O} + \text{H}]^+$ fragment peaks for all long-chain SM molecular species eluted in SL2. On the other hand, the short-chain DSM species that

Table 1
Semi-quantitative estimations of bovine milk sphingolipid molecular species based on APCI-MS data

FA	DSM							SM				
	12:0 ^a	14:0	16:0	17:0	18:0	19:0	20:0	16:1	17:1	18:1	19:1	20:1
FA	0.25 ^b	0.42	0	56.09	5.24	36.47	0.98	26.03	10.52	60.23	2.98	0.24
10:0										0.02		
12:0					0.03 ^c					0.02		
13:0					0.13					0.01		
14:0	0.12		0.19		0.30			0.14	0.12	0.80		
14:1										0.12		
15:0				0.09	0.28				0.01	0.17		
15:1										0.15		
16:0		0.05	4.19	1.00	5.74	0.45	0.17	2.30	2.15	12.88	0.48	
16:1										0.28		
17:0			0.10		0.03			0.06		0.48		
17:1										0.11		
18:0			0.77	0.06	0.64			0.38	0.24	0.83	0.07	
18:1										0.30		
19:0			0.07		0.04					0.08		
20:0			0.19		0.14			0.13	0.04	0.26		
20:1					0.96					0.47		
21:0			0.67		0.14			0.22	0.11	0.33		
21:1					3.47					0.07		
22:0			13.04	0.78	4.09			4.56	1.48	8.94	0.30	
22:1					4.11				0.06	0.07		
23:0	0.14	0.37	22.84	2.05	8.02	0.32	0.24	9.22	2.98	16.02	0.21	0.24
23:1					2.38			1.33	0.49	1.61	0.46	
24:0			14.02	1.27	4.08	0.20	0.14	5.15	2.31	11.62	1.19	
24:1					1.33			1.40	0.35	2.06	0.26	
25:0					0.19			0.19	0.19	0.88		
25:1					0.32			0.61		0.87		
26:0					0.06			0.33		0.48		
26:1										0.32		
	DSM Total = 100.01							SM Total = 100.01				
	DSM = 20.8% of SLs							SM = 79.2% of SLs				

^a Numbers represent the identities of the long-chain bases within the SL class, given as carbon chain length: sites of unsaturation.

^b Values represent the percentage of each long-chain base in the SL class.

^c Values represent the percentage of each fatty amide chain combined with each long-chain base in the SL class.

also eluted in SL2 gave larger [Cer-H₂O+H]⁺ peaks than [Cer-2H₂O+H]⁺ peaks, similar to the trend for long-chain DSM species in SL1. The combination of the [Cer-H₂O+H]⁺ peaks in the mass range *m/z* 450–550 with the [Cer-H₂O+H]⁺ and [Cer-2H₂O+H]⁺ peaks in the mass range *m/z* 550–650 demonstrated that short-chain DSM species and long-chain SM species were overlapped in SL2, in agreement with our previous reports. The distinctive masses, as well as the differences between the ratios of the [Cer-H₂O+H]⁺ peaks to the [Cer-2H₂O+H]⁺ peaks, served to differentiate these two classes of sphingolipids.

If the *m/z* values of the [Cer-H₂O+H]⁺ and [Cer-2H₂O+H]⁺ pairs of peaks in the *m/z* 550–650 range given above were to correspond to SM species having all 18-carbon LCBs, they would correspond to *d*18:1/24:0, *d*18:1/23:0, *d*18:1/22:0, *d*18:1/21:0, and *d*18:1/20:0, respectively. However, the *m/z* 200–300 range in the full-scan APCI-MS spectrum in Fig. 1C provided direct evidence that several LCBs in addition to the *d*18:1 LCB were present in milk SLs. Although the *m/z* 264.4 peak in Fig. 1C indicated that the largest abundance of SM species had the *d*18:1 LCB (approximately 60.2%, as given in Table 1), the peak at *m/z*

236.4 indicated that the *d*16:1 long-chain base was the second most abundant LCB (26.0%), the peak at *m/z* 250.4 indicated that some species contained the *d*17:1 LCB (10.5%), the peak at *m/z* 278.4 indicated that some species contained the *d*19:1 LCB (3.0%), and there was a very small amount of species having the *d*20:1 LCB (0.2%) which gave a small peak at *m/z* 292.4. These identities were confirmed by the MS/MS and MS³ data, as discussed below. The LCB fragments from SM species in Fig. 1C gave larger abundances, as a proportion to the ceramide-related fragments, than the long-chain base fragments from the DSM species shown in Fig. 1B.

In the full-scan spectrum in Fig. 1C, the fragments in the range *m/z* 320–420 arose from the fatty amide chain portion of the SM molecules. The ions at *m/z* 364.6, *m/z* 378.6, and *m/z* 392.6 are referred to as the [FA(long)]⁺ fragments, and indicated the presence of 22:0, 23:0 and 24:0 FA chains. The molecular species containing these FA chains also gave the corresponding [FA(short)]⁺ fragments at *m/z* 340.5, *m/z* 354.5, and *m/z* 368.5, respectively. The combination of the [FA(long)]⁺ and [FA(short)]⁺ fragments, separated by 24 *m/z*, provided mutual confirmation of the 22:0, 23:0 and 24:0 FA chains. MS/MS spec-

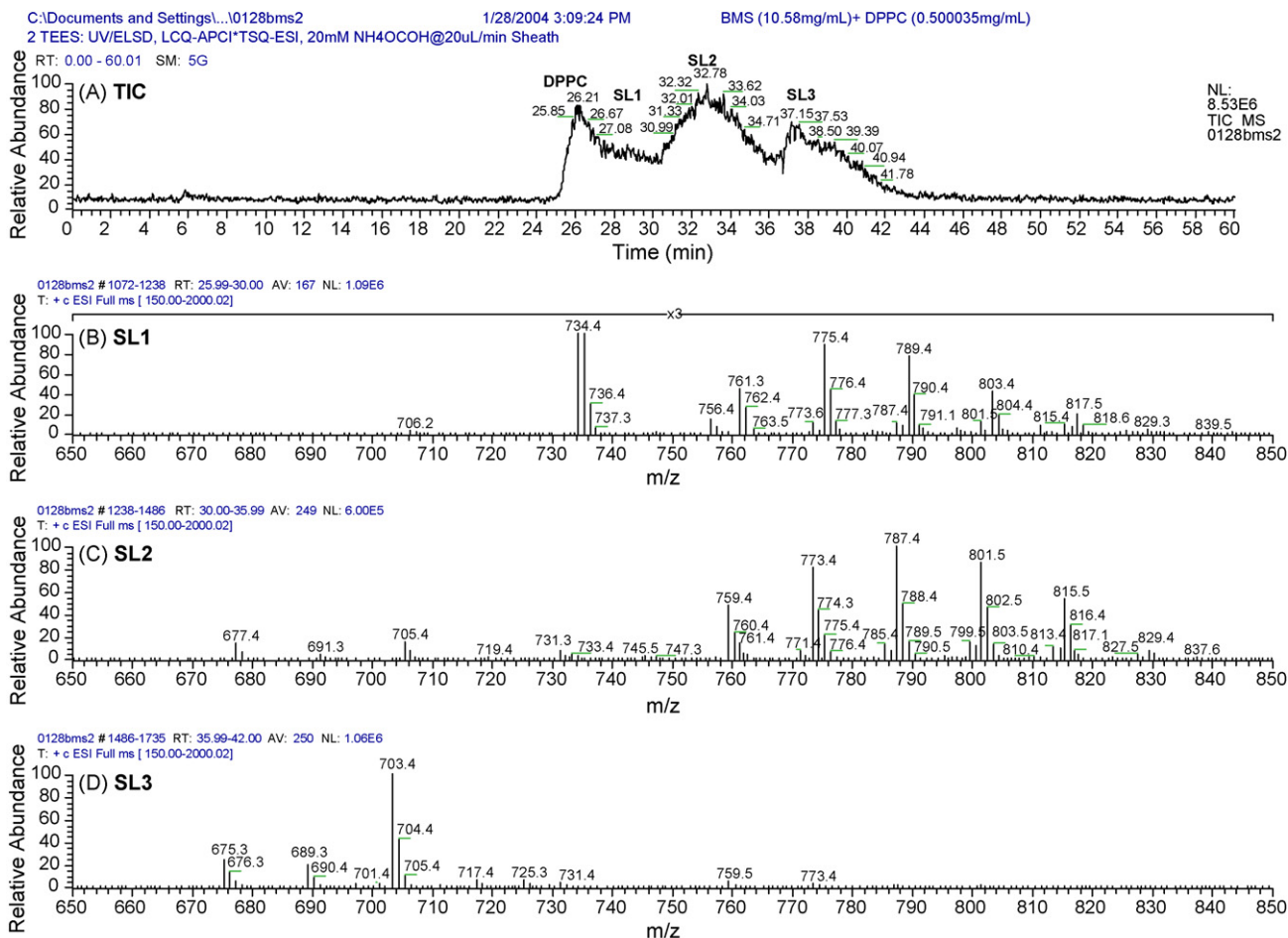


Fig. 2. ESI-MS total ion current chromatogram and full-scan mass spectra. (A) TIC; (B) averaged mass spectrum across sphingolipid peak 1, SL1, from 26 to 30 min; (C) averaged mass spectrum across SL2, from 30 to 36 min; (D) averaged mass spectrum across SL3, from 36 to 42 min. Obtained in parallel with run shown in Fig. 1.

tra also showed the $[FA(\text{long})]^+$ and $[FA(\text{short})]^+$ fragments, and allowed further confirmation of all of the fatty amide chains identified and estimated in Table 1.

Fig. 1D shows the fragments that came from SLs eluted in the third sphingolipid peak, SL3. The $[Cer-H_2O+H]^+$ peaks at m/z 534.4, m/z 520.4, m/z 506.4, and m/z 492.4 showed elution of short-chain SM species, which gave corresponding $[Cer-2H_2O+H]^+$ peaks at m/z 516.5, m/z 502.6, m/z 488.5, and m/z 474.5, respectively. If the m/z values of the $[Cer-H_2O+H]^+$ and $[Cer-2H_2O+H]^+$ pairs of peaks in Fig. 1D were to correspond to SM species having all 18-carbon LCBs, they would correspond to $d18:1/17:0$, $d18:1/16:0$, $d18:1/15:0$, and $d18:1/14:0$, respectively. However, the full-scan APCI-MS spectrum in Fig. 1D showed the same LCB fragment ions in the range m/z 200–300 as Fig. 1C, which provided direct evidence that several LCBs in addition to the $d18:1$ LCB were present in milk SLs. The $[FA(\text{long})]^+$ fragment at m/z 280.4, which arose from the 16:0 FA of $d18:1/16:0$, was larger than the $[LCB-H_2O]^+$ ion at m/z 278.4 from the 19:1 LCB because $d18:1/16:0$ was the most abundant short-chain SM. The FAs identified in the full-scan spectra were confirmed by the MS/MS data discussed below, and an estimate of their composition is given with the estimated composition of LCBs in Table 1.

3.2. Full-scan ESI-MS mass spectra

The ESI-MS data obtained from BMS shown in Fig. 2 were obtained simultaneously in parallel from the same column eluate as the APCI-MS data given in Fig. 1. In Fig. 2A, the peak that arose from the 0.5 mg/mL of dipalmitoyl glycerophosphocholine internal standard (see Experimental section) showed higher response than the SLs, as discussed in our recent report [28]. Fig. 2B was scaled to full height for maximum visibility of the long-chain DSM species, so the peak at m/z 734.4 was allowed to go off scale. Because dipalmitoyl glycerophosphocholine gave such strong response, its $[M+Na]^+$ adduct ion is also observed at m/z 756.4. In contrast, the APCI-MS spectrum in Fig. 1B showed only small peaks at m/z 551.5 and m/z 734.3 for the dipalmitoyl fragment ion, $[PP]^+$, and the protonated molecule from dipalmitoyl glycerophosphocholine, respectively, as previously discussed [28]. ESI-MS/MS of $[M+H]^+$ ions of SLs gave almost exclusively the phosphocholine head group fragment at m/z 184.1, which is not structurally informative, as has been reported in the past [33,37]. Therefore, no ESI-MS/MS data are presented.

Fig. 2B showed the protonated molecules for all of the molecular species discussed above that were identified by APCI-

Table 2
Semi-quantitative estimations of bovine milk sphingolipid molecular species based on ESI-MS data

FA	DSM							SM				
	12:0 ^a	14:0	16:0	17:0	18:0	19:0	20:0	16:1	17:1	18:1	19:1	20:1
FA	0.27	0.39	0	58.39	5.42	34.06	0.91	29.59	11.09	57.34	1.86	0.11
10:0										0.03		
12:0					0.06					0.05		
13:0					0.15					0.01		
14:0	0.15		0.43		0.58			0.34	0.30	1.60		
14:1										0.07		
15:0				0.17	0.43				0.02	0.33		
15:1										0.09		
16:0		0.11	8.05	1.53	7.12	0.42	0.21	4.60	4.12	23.70	0.54	
16:1										0.70		
17:0			0.16		0.02			0.12		0.54		
17:1										0.11		
18:0			0.95	0.06	0.81			0.69	0.27	1.40	0.11	
18:1										0.40		
19:0			0.06		0.03					0.13		
20:0			0.24		0.17			0.22	0.06	0.38		
20:1					0.37					0.18		
21:0			0.51		0.13			0.34	0.16	0.34		
21:1					3.13					0.05		
22:0			14.96	0.69	3.71			6.73	1.53	7.05	0.19	
22:1					2.54				0.04	0.06		
23:0	0.13	0.28	20.32	1.86	7.05	0.28	0.25	9.50	2.35	9.99	0.12	0.11
23:1					2.37			1.02	0.42	1.24	0.22	
24:0			12.71	1.12	3.58	0.21	0.09	4.06	1.44	6.78	0.57	
24:1					1.10			1.20	0.27	1.00	0.11	
25:0					0.19			0.12	0.11	0.42		
25:1					0.49			0.47		0.37		
26:0					0.04			0.19		0.24		
26:1										0.07		
	DSM Total = 100.02 DSM = 19.8% of SLs							SM Total = 99.99 SM = 80.2% of SLs				

^a See footnotes in Table 1.

MS. The primary $[M+H]^+$ peaks in Fig. 2B were at m/z 761.3, m/z 775.4, m/z 789.4, m/z 803.4, and m/z 817.5. If these all had 18-carbon long-chain bases, they would correspond to $d18:0/20:0$, $d18:0/21:0$, $d18:0/22:0$, $d18:0/23:0$, and $d18:0/24:0$, respectively. These were the same species identified by the $[\text{Cer-H}_2\text{O}+H]^+$ and $[\text{Cer-2H}_2\text{O}+H]^+$ fragments obtained by APCI-MS, and showed that the ESI-MS data obtained using the 'dual parallel' approach provided valuable molecular weight information that confirmed the identification of molecular species based on fragments in APCI-MS spectra. Similarly, the $[M+H]^+$ peaks at m/z 705.4, m/z 691.3, and m/z 677.4 in Fig. 2C showed elution of the short-chain DSM species $d18:0/16:0$, $d18:0/15:0$, and $d18:0/14:0$, respectively, along with their isobaric counterparts having other saturated long-chain bases. Peaks with similar masses were evident in a previous report [37], but were not mentioned or discussed. Thus, the previous report did not identify short-chain DSM species overlapped with long-chain SM species in SL2. Here, we have provided APCI-MS, MS/MS and ESI-MS data to show that these were short-chain DSM species, in agreement with our previous reports [29,34].

The $[M+H]^+$ peaks in the range m/z 730–850 and the SM molecular species they represented were as follows (based on

having all 18-carbon LCBs): m/z 731.3 ($d18:1/18:0$), m/z 745.5 ($d18:1/19:0$), m/z 759.4 ($d18:1/20:0$), m/z 773.4 ($d18:1/21:0$), m/z 787.4 ($d18:1/22:0$), m/z 801.5 ($d18:1/23:0$), m/z 815.5 ($d18:1/24:0$), and m/z 829.4 ($d18:1/25:0$). Of course, all molecular species did not have $d18:1$ long-chain base backbones, so the observed masses represented the isobaric combinations of monounsaturated LCBs with saturated fatty amides. The $d18:1$ LCB was estimated to constitute approximately 57.3% of the total monounsaturated LCBs determined by ESI-MS, as given in Table 2. This compared well to the 60.2% estimated by APCI-MS, given in Table 1. The $d16:1$ LCB was the second most abundant SM LCB determined by ESI-MS, representing approximately 29.6% of the SM LCBs, also in fair agreement with the APCI-MS data.

The average full-scan ESI-MS mass spectrum across SL3 of milk SLs is given in Fig. 2D. The $[M+H]^+$ peaks and the SM molecular species that they represented were as follows (based on having all 18-carbon LCBs): m/z 675.3 ($d18:1/14:0$), m/z 689.3 ($d18:1/15:0$), m/z 703.4 ($d18:1/16:0$), and m/z 717.4 ($d18:1/17:0$). These identifications agree with the identifications based on the APCI-MS data presented in Fig. 1D. The complete composition of isobaric species having different combinations of LCBs and FAs estimated from ESI-MS data is given in Table 2.

Semi-quantitative analysis based on the relative peak areas of all DSM and SM species determined by APCI-MS indicated that BMS were composed of 21% DSM species and 79% SM species. Based on the relative peak areas of all DSM and SM species determined by ESI-MS, BMS were composed of 20% DSM species and 80% SM species. This was surprisingly good agreement between these two very different ionization modes, one which used the sum of two fragments for quantification, and the other which used only the protonated molecules. Both of these HPLC/atmospheric pressure ionization (API)-MS techniques gave slightly higher percentages of DSM than that reported by Morrison and Hay, which was 17.8%, with 82.2% SM [21]. These DSM percentages were also higher than were obtained from the percentage composition determined by ^{31}P NMR, discussed below, which was 16.2% DSM and 83.8% SM. Nevertheless, it was obvious from both of these HPLC/API-MS techniques that substantial proportions of DSM species were present and the molecular species could be identified using APCI-MS and ESI-MS.

3.3. APCI-MS, MS/MS and MS^3 mass spectra

Fig. 3 shows the APCI-MS, MS/MS and MS^3 spectra averaged across the peak that corresponded to the isobaric species $d16:0/23:0$, $d17:0/22:0$ and $d18:0/21:0$. These species eluted in SL1 (Fig. 1), between 27.5 and 31 min, and gave primarily the $[\text{Cer-H}_2\text{O} + \text{H}]^+$ fragment at m/z 592.7 in the average mass spectrum shown in Fig. 3B, although small abundances of $[\text{M} + \text{H}]^+$ at m/z 775.4 and $[\text{M} + \text{Na}]^+$ at m/z 797.4 were observed. The MS^n mass spectra in Fig. 3 allowed the composition of the isobaric molecular species to be determined. The spectral region from m/z 230 to m/z 290, expanded in the MS/MS spectrum, Fig. 3D, of the m/z 592.7 precursor contained all of the $[\text{LCB}]^+$ and $[\text{LCB-H}_2\text{O}]^+$ fragments that allowed the sphingolipid backbones to be identified. The largest fragments were observed at m/z 256.2 and m/z 238.2, which represented the $[\text{LCB}]^+$ and $[\text{LCB-H}_2\text{O}]^+$ fragments, respectively, from the $d16:0$ LCB. These two fragments, considered together with the m/z 592.7 $[\text{Cer-H}_2\text{O} + \text{H}]^+$ precursor ion and the m/z 574.5 $[\text{Cer-2H}_2\text{O} + \text{H}]^+$ fragment ion indicated a $d16:0/23:0$ sphingolipid structure. This identity was confirmed by the $[\text{FA}(\text{short})]^+$ and $[\text{FA}(\text{long})]^+$ fragments at m/z 354.4 and m/z 378.4, respectively, in Fig. 3C, and at m/z 354.3 and m/z 378.3, respectively, in the APCI- MS^3 spectrum in Fig. 3E. The second most abundant pair of $[\text{LCB}]^+$ and $[\text{LCB-H}_2\text{O}]^+$ diagnostic ions in Fig. 3D were at m/z 270.2 and m/z 252.2, respectively, which represented the $d17:0$ LCB. Considered together with the m/z 592.7 precursor ion and the m/z 574.5 $[\text{Cer-2H}_2\text{O} + \text{H}]^+$ fragment ion, these indicated a $d17:0/22:0$ sphingolipid structure. This identity was confirmed by the $[\text{FA}(\text{short})]^+$ fragment at m/z 340.4 in the MS/MS spectrum in Fig. 3C and at m/z 340.3 in Fig. 3E and the $[\text{FA}(\text{long})]^+$ fragment m/z 364.2 in the MS^3 mass spectrum in Fig. 3E. Finally, a small amount of the LCB $d18:0$ was indicated by the presence of the $[\text{LCB}]^+$ fragment at m/z 284.3 and $[\text{LCB-H}_2\text{O}]^+$ at m/z 266.3 in Fig. 3D, which considered with the m/z 592.7 $[\text{Cer-H}_2\text{O} + \text{H}]^+$ ion and the m/z 574.5 $[\text{Cer-2H}_2\text{O} + \text{H}]^+$ fragment ion indicated a $d18:0/21:0$ sphingolipid

structure. A small abundance of m/z 350.1 in Fig. 3E that represented the $[\text{FA}(\text{long})]^+$ fragment of the $21:0$ FA confirmed that a small amount of this isobaric species was present. Tables 1 and 2 show that the $d16:0/23:0$ DSM species was estimated to be the most abundant of the DSM species. The $d17:0/22:0$ molecular species represented less than 1% of the DSM species, while the $d18:0/21:0$ represented less than 0.2% of the DSM species. The identities of all species were confirmed by the presence of an intact $[\text{M} + \text{H}]^+$ ion in the full scan ESI-MS mass spectrum, as well as by ESI- MS^n data (not shown).

There were other molecular species that were isobaric with the species mentioned above. One was the $2 \times ^{13}\text{C}$ isotopic variant of $d18:0/21:1$, which represented $\sim 3.5\%$ of DSM species. The calculated monoisotopic mass of $d18:0/21:1$ was 773.7 Da. A certain percentage of the population of molecules contained one ^{13}C isotope or one ^2H deuterium isotope, and a smaller proportion of the population contained two ^{13}C isotopes or one ^{13}C isotope and a ^2H deuterium isotope. Only those species containing two isotopes are of concern, since the $2 \times ^{13}\text{C}$ isotopic variant of $d18:0/21:1$ was isobaric with the monoisotopic variant of $d16:0/23:0$. The presence of isotopic variants was discussed in great detail in our previous report [28], and is mentioned further below. More importantly, the effect of another isotopic variant also having the $[\text{Cer-H}_2\text{O} + \text{H}]^+$ fragment at m/z 592.7 is seen in Fig. 3A. The $2 \times ^{13}\text{C}$ isotope variant or the $1 \times ^{13}\text{C}$ isotope plus $1 \times ^2\text{H}$ deuterium isotope variant of $d16:1/23:0$ is isobaric with $d16:0/23:0$ and the other species mentioned above. Both these species gave a m/z 775.4 $[\text{M} + \text{H}]^+$ ion by ESI-MS and a m/z 592.7 base peak by APCI-MS. However, the $2 \times ^{13}\text{C}$ isotope variant (or the $1 \times ^{13}\text{C}$ isotope plus $1 \times ^2\text{H}$ deuterium isotope variant) of $d16:1/23:0$ was chromatographically resolved from monoisotopic $d16:0/23:0$, since the former is a long-chain SM and eluted in SL2, while the latter is a long-chain DSM species and eluted in SL1. The peak in Fig. 3A that eluted between 31.5 and 35 min is the isotopic variant of $d16:1/23:0$, and is labeled with an 'X' to indicate that it should not be confused with the normal, monoisotopic species. If not properly recognized, the isotopic variants can be confused with isobaric monoisotopic species, leading to misidentification of molecular species.

The data in Fig. 3 provided one example of how several isobaric SLs that gave the same $[\text{Cer-H}_2\text{O} + \text{H}]^+$ and $[\text{Cer-2H}_2\text{O} + \text{H}]^+$ fragments, but having different LCBs and FA combinations, were differentiated based on their $[\text{LCB}]^+$, $[\text{LCB-H}_2\text{O}]^+$, $[\text{FA}(\text{long})]^+$ and $[\text{FA}(\text{short})]^+$ fragments. Repeating this process using APCI-MS, MS/MS and MS^3 spectra for every peak in the average mass spectrum across each of the three sphingolipid peaks allowed the full range of DSM and SM species to be identified.

3.4. ^{31}P NMR spectroscopy

Fig. 4 shows that ^{31}P NMR spectroscopy gave a strong resonance signal at 0.13 δ that corresponded to dihydrosphingomyelin in the commercially available BMS sample. Quantitative analysis based on the integrated areas from the average of three ^{31}P NMR spectra indicated that BMS was composed of $16.20 \pm 0.27\%$ DSM and $83.80 \pm 0.27\%$ SM. Thus,

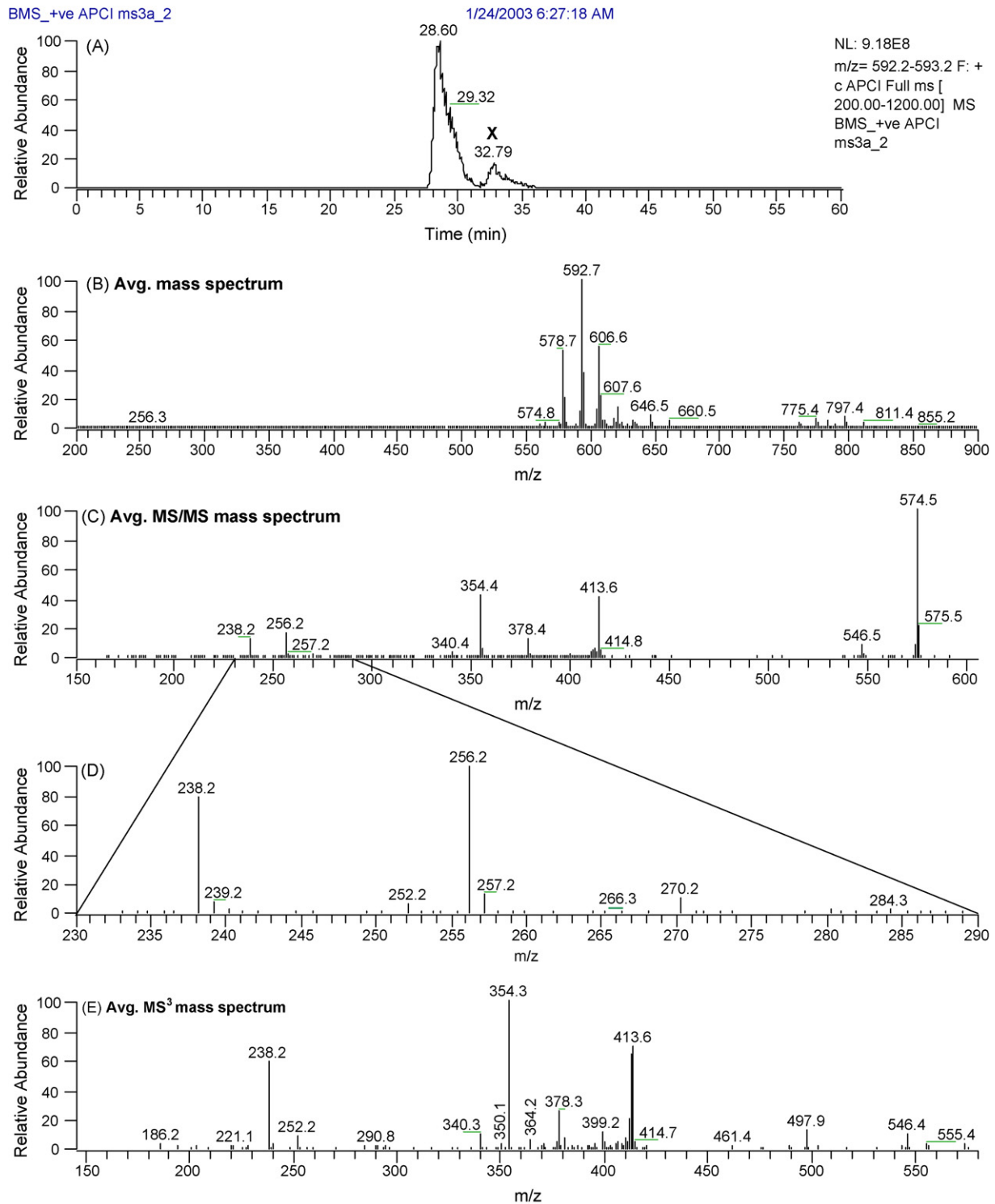


Fig. 3. (A) EIC of APCI-MS, MS/MS and MS³ scans of m/z 592.7, which represents several isobaric species of DHS; (B) Mass spectrum averaged from 28–30 min in (A); (C) average MS/MS mass spectrum of m/z 592.7; (D) m/z 230–290 region of MS/MS mass spectrum showing LCB fragments; and (E) MS³ scan of m/z 592.7 \rightarrow m/z 574.5. Not run in parallel.

DSM represented a higher proportion of SL in BMS than in bovine brain SM. Previously, Morrison [22] and Morrison and Hay [21] had reported derivatization of BMS SLs to form their dinitrophenyl (DNP) derivatives, followed by conversion to aldehydes by periodate and analysis of the aldehydes using

gas–liquid chromatography (GLC) with flame ionization detection (FID). They reported a composition of 17.8% saturated LCB species (DSM) and 82.2% monounsaturated long-chain base species (SM). Thus, our results are in better agreement with older reports than with other HPLC/API-MS methods

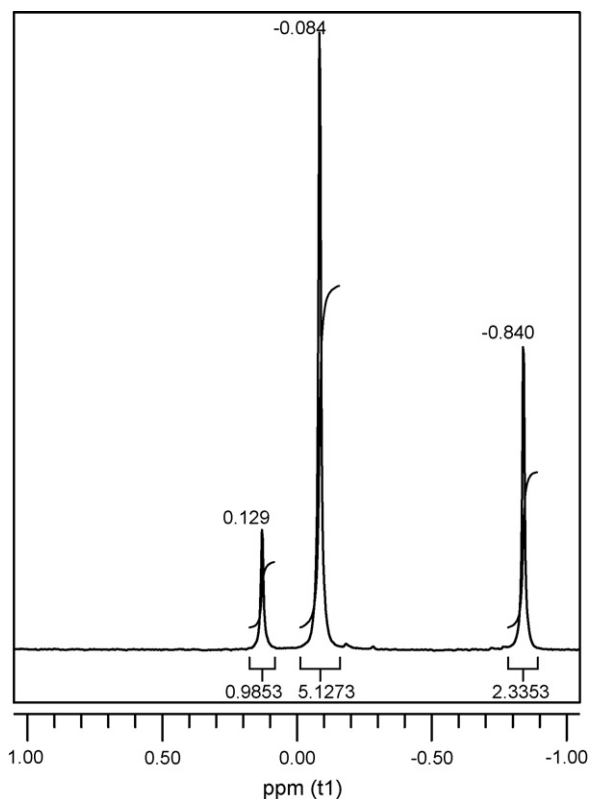


Fig. 4. ^{31}P NMR spectrum of bovine milk sphingolipids (25.3 mg/mL) with dipalmitoyl glycerophosphocholine as internal standard (10.6 mg/mL) and chemical shift axis reference.

cited below which did not report substantial proportions of DSM species. Quantification of the absolute amounts of SLs in BMS from three runs, by comparison to the internal standard, gave absolute amounts of 4.47, 5.35 and 4.59 mg/mL for an average of 4.80 ± 0.48 mg/mL of DSM, and 23.27, 27.09 and 24.14 mg/mL for an average of 24.84 ± 2.00 mg/mL of SM. The sum of these values was 29.64 mg/mL of SL. The actual average amount of BMS in the analyzed samples was 26.6 mg/mL. Thus, the absolute amounts of SLs determined by ^{31}P NMR were higher than the known amounts present, presumably due to the different response of the dipalmitoyl glycerophosphocholine internal standard versus the DSM and SM classes. Nevertheless, ^{31}P NMR spectroscopy confirmed the results obtained by online HPLC/APCI-MS and HPLC/ESI-MS that indicated that commercially available bovine milk sphingomyelin contained a substantial proportion of dihydrosphingomyelin in addition to sphingomyelin.

3.5. Negative-ion ESI-MS mass spectra

There is a paucity of data extant in the literature showing negative-ion API mass spectra of sphingolipids. Kerwin et al. [33] reported quantification of several phospholipids classes including bovine brain SLs by both positive- and negative-ion ESI-MS, but no mass spectra of SLs were presented. Han and Gross [35] showed an ESI-MS/MS mass spectrum of the chlorine adduct of $d18:1/18:0$ SM in negative ion mode. Both

reports used a sample infused into the source without chromatographic separation. The results presented here represent important precedent showing ESI-MS and APCI-MSⁿ coupled online to NP-HPLC to obtain negative-ion mass spectra of chromatographically resolved intact sphingolipid classes. The ESI-MS and APCI-MS results in negative-ion mode were both obtained on the ITMS instrument (see Experimental section) and the parallel runs in positive-ion mode on the TSQ are not presented since they duplicate results discussed above.

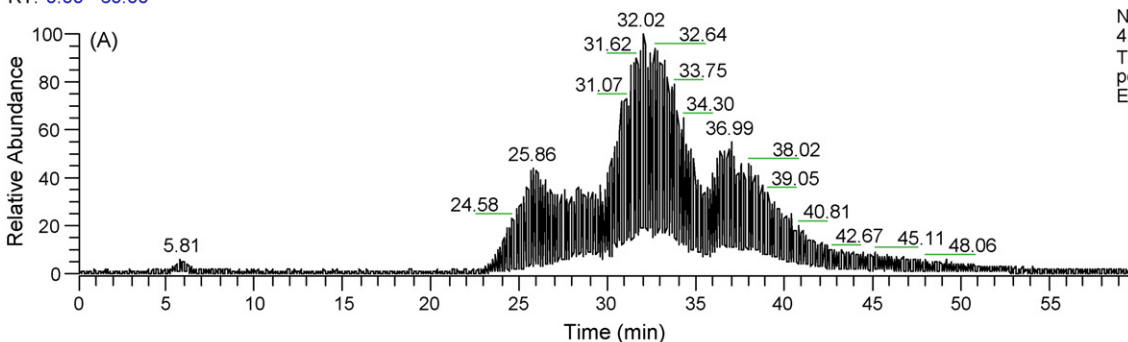
Fig. 5 shows the TIC and ESI-MS mass spectra averaged across each of the three SL peaks. ESI-MS produced virtually exclusively formate adducts, with no other fragments or ions apparent above the 1% label threshold. Therefore, only the m/z 650 to 950 region of the mass spectra, which contain the formate adducts, are shown in Fig. 5B–D. Sphingomyelin is naturally a zwitterionic molecule, having a (+) charge on the quaternary amine and a (–) charge on a phosphate oxygen. The zwitterionic form is usually referred to as ‘M’, so the ion that has a proton on a phosphate oxygen is referred to as the protonated molecule, $[\text{M} + \text{H}]^+$. Therefore, the ion formed by association of a formate anion, HCOO^- , with the quaternary amine of the zwitterionic molecule, M, to leave a net negative charge on a phosphate oxygen is referred to as $[\text{M} + \text{HCOO}]^-$, or $[\text{M} + 45]^-$. The structure of the formate adduct attached to the phosphocholine head group is shown inset in Fig. 5D. Formation of the formate adduct with another phosphocholine-containing phospholipid, platelet activating factor (acetyl-*O*-hexadecyl glycerophosphocholine), was shown previously by Kerwin et al. [33]. Similarly, Uran et al., among others, identified glycerophosphocholine, lyso-glycerophosphocholine and SM as formate adducts [36]. Fig. 5B showed the formate adducts of the long-chain DSM species that corresponded to the same long-chain species that were identified by their positive-ion APCI-MSⁿ and ESI-MS mass spectra presented above. The major ions at m/z 805.6, m/z 819.5, m/z 833.5 and m/z 847.5 corresponded to $d18:0/20:0$, $d18:0/21:0$, $d18:0/22:0$, $d18:0/23:0$, respectively, which were isobaric with $d17:0/21:0$, $d17:0/22:0$, $d17:0/23:0$, $d17:0/24:0$, respectively, and with $d16:0/22:0$, $d16:0/23:0$, $d16:0/24:0$, $d16:0/25:0$ (not observed), respectively. The molecular species identified by these negative ions corresponded exactly with the species identified using the $[\text{M} + \text{H}]^+$ ions by positive-ion ESI-MS and the $[\text{Cer-H}_2\text{O} + \text{H}]^+$ and $[\text{Cer-2H}_2\text{O} + \text{H}]^+$ ions observed by positive-ion APCI-MS, providing another valuable means for confirmation of the presence of long-chain DSM species in SL1. The ion at m/z 778.5 was the formate adduct from the dipalmitoyl glycerophosphocholine internal standard, since it also contained a phosphocholine head group that formed the same type of $[\text{M} + 45]^-$ adduct.

The ions in the range m/z 800 to 900 in Fig. 5C were 2 m/z lower than those in Fig. 5B, reflecting the 4,5-*trans* site of unsaturation that distinguishes SM species from DSM species. Thus, the major ions at m/z 803.5, m/z 817.6, m/z 831.5 and m/z 845.5 corresponded to $d18:1/20:0$, $d18:1/21:0$, $d18:1/22:0$, $d18:1/23:0$, respectively, which were isobaric with $d17:1/21:0$, $d17:1/22:0$, $d17:1/23:0$, $d17:1/24:0$, respectively, and with $d16:1/22:0$, $d16:1/23:0$, $d16:1/24:0$, $d16:1/25:0$, respectively.

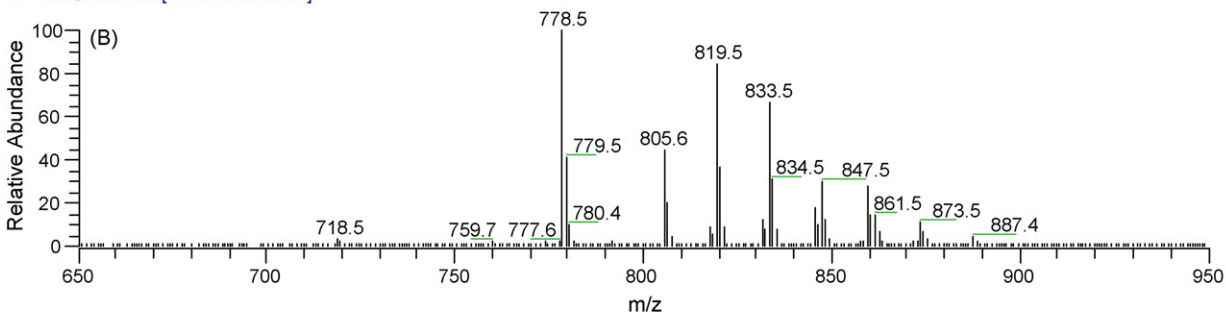
BMS pos-neg ESI_1
RT: 0.00 - 60.00

2/18/2004 12:31:59 AM

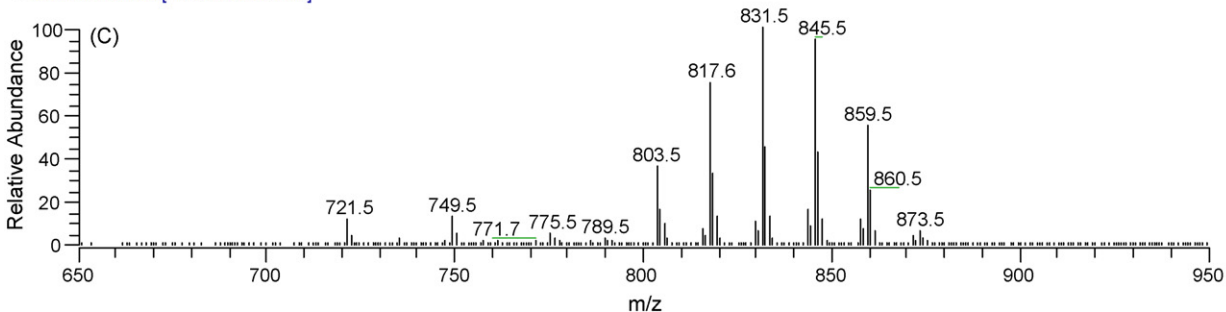
NL:
4.90E9
TIC MS BMS
pos-neg
ESI_1



BMS pos-neg ESI_1 # 597-724 RT: 25.02-30.01 AV: 64 NL: 3.21E7
T: - c ESI Full ms [170.00-2000.00]



BMS pos-neg ESI_1 # 724-863 RT: 30.01-35.45 AV: 70 NL: 6.16E7
T: - c ESI Full ms [170.00-2000.00]



BMS pos-neg ESI_1 # 863-1027 RT: 35.53-41.98 AV: 82 NL: 9.03E7
T: - c ESI Full ms [170.00-2000.00]

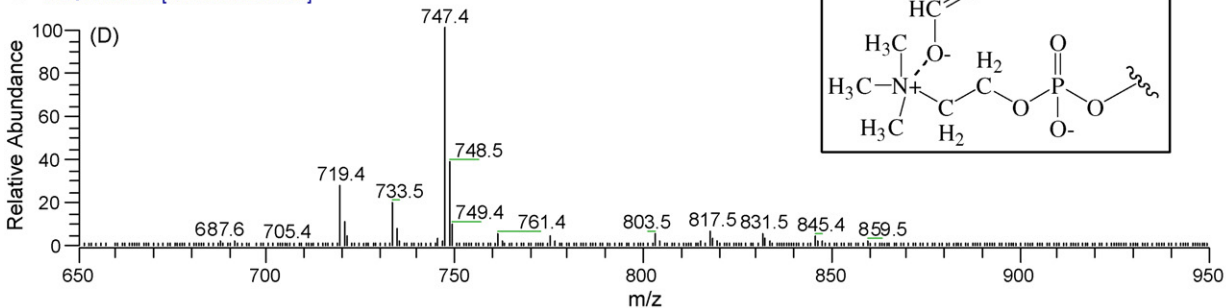


Fig. 5. Negative-ion ESI-MS data for BMS. (A) TIC showing alternating positive and negative scans; (B) average negative-ion mass spectrum across SL1, from 25 to 30 min; (C) average negative-ion mass spectrum across SL2, from 30 to 35.5 min; (D) average negative-ion mass spectrum across SL3, from 35.5 to 42 min. Structure of formate adduct, $[M + \text{HCOO}]^- = [M + 45]^-$ inset. Parallel (+) APCI-MS run on TSQ not shown.

These corresponded exactly to the SM species identified in positive-ion mode, discussed above. The ions at m/z 721.5 and m/z 749.5 in Fig. 5C corresponded to $d16:0/16:0$ and $d16:0/18:0$, respectively, which were isobaric with $d17:0/15:0$

and $d17:0/17:0$, respectively and $d18:0/14:0$ and $d18:0/16:0$, respectively. These ions provided valuable data for confirmation that short-chain DSM species occurred overlapped with long-chain SM species in SL2.

The largest two ions in Fig. 5D, m/z 719.4 and m/z 747.4, were at 2 m/z lower than the ions just mentioned in the low-mass portion of the spectrum of Fig. 5C, reflecting the presence of the 4,5-*trans* site of unsaturation that distinguishes short-chain SM species eluted in SL3 from the short-chain DSM species that eluted in SL2. The formate adduct ions at m/z 719.4, m/z 733.5 and m/z 747.4 identified the SM species $d16:1/16:0$, $d16:1/17:0$ and $d16:1/18:0$, respectively, which were isobaric with $d17:1/15:0$, $d17:1/16:0$ and $d17:1/17:0$, respectively, and also isobaric with $d18:1/14:0$, $d18:1/15:0$ and $d18:1/16:0$, respectively. These adducts provide additional data to confirm the identification of short-chain SM species in SL3 that were identified based on the positive-ion MS data given above and listed in Tables 1 and 2.

3.6. Negative-ion APCI-MS mass spectra

The negative-ion APCI-MS data show some important differences from the negative-ion ESI-MS mass spectra that must be understood to avoid misidentification of SL molecular species. Fig. 6 represents the first example of negative-ion APCI-MS coupled online to NP-HPLC for identification of SM and DSM classes. The first two observations regarding (–) APCI-MS mass spectra compared to (–) ESI-MS mass spectra are: (1) the spectra are substantially more complicated, with more fragments evident; and (2) the formate adducts appear at 2 m/z lower than they did in the (–) ESI-MS spectra. Thus, it is not actually a formate adduct, but a modified formate adduct, or a formate-like adduct that appears in (–) APCI-MS spectra. The formate moieties are not simply loosely associated with the quaternary amine head group, but rather the higher energy present in the plasma at the tip of the corona discharge needle of the APCI source, compared to an ESI source, caused a higher-energy covalent association of the formate moiety with the choline head group. We could get a good idea about the nature of this stronger association by examining the second most abundant fragment that was formed. The $[M - 15]^-$ fragment ion was the second most abundant after the formate-like adduct. The $[M - 15]^-$ fragment has been reported before for sphingolipids [35,37], as well as glycerophosphocholines, and represents loss of a methyl group, $-\text{CH}_3$, from the quaternary amine, causing it to lose the quaternary (+) charge and become simply an *N,N*-dimethyl tertiary amine. The remaining (–) charge on the phosphate group allows the fragment to show up quite well by negative-ion ESI-MS or APCI-MS. If the formate-like adduct were bonded to one of the ethanolamine carbons, it would be expected to lose the whole choline portion of the head group or a larger portion of it, instead of only one of the methyl groups from the amine. Therefore, it is more likely that the formate group forms a linkage to one of the choline methyl groups, making it a better leaving group, and leading to enhanced formation of the $[M - 15]^-$ fragment, which is observed. The proposed structure of the formate-like ion is shown inset in Fig. 6, but definitive confirmation of its structure awaits deuterium-labeled experiments to elucidate exactly which two hydrogens are lost during bonding of the formate to the head group.

Since DSM and SM differ by only 2 m/z , it is important to recognize that negative-ion APCI-MS mass spectra differ from ESI-MS for a reason that is completely unrelated to differences in the structures of the molecules themselves, but instead is due to a difference in the energy of ionization within the two ionization sources and so the nature of the adduct formed. It is important to recognize that both classes of SLs, DSM and SM, exhibit the same difference of 2 m/z observed in (–) APCI-MS spectra (Fig. 6) compared to (–) ESI-MS spectra (Fig. 5). Once this is realized, the difference of 2 m/z due to the difference in SL structures can still be recognized. The primary DSM species in Fig. 6B appeared at m/z 803.6, m/z 817.6, m/z 831.6 and m/z 845.5, while the primary SM species in Fig. 6C appeared at masses 2 m/z lower, at m/z 801.6, m/z 815.5, m/z 829.5 and m/z 843.5. Without understanding this important difference between the formate adduct formed by ESI-MS and the formate-like adduct formed by APCI-MS in negative-ion mode, the peaks in SL1 at m/z 803.6, m/z 817.6, m/z 831.6 and m/z 845.5 could easily be mistaken for long-chain SM species, since they have the same masses as the formate adducts shown in Fig. 5C, but actually arise from DSM species instead of SM species. This is another example of how the chromatographic separation of SLs into the classes of DSM and SM allows ambiguity leading to potential misidentification to be avoided.

As would be expected from the discussion above, the formate-like adduct ions in the negative-ion APCI-MS mass spectrum averaged across SL3, shown in Fig. 6D, were at 2 m/z lower than the same molecular species observed by negative-ion ESI-MS, shown in Fig. 5D. In contrast to the formate-like adducts, the $[M - 15]^-$ fragments shown in all spectra in Fig. 6 are the same as those produced by ESI-MS/MS [35,37] and are not further discussed here. Masses of these ions are given at www.sphingomyelin.com. Another important observation is that the $[M + 43]^-$ formate-like adduct is not formed totally to the exclusion of the normal formate adduct. Examination of mass spectra in Fig. 6 showed that the peak at 2 m/z higher than the masses discussed above, *i.e.* at the masses for normal formate adducts, were present at abundances that are higher than would be expected due solely to the $2 \times {}^{13}\text{C}$ isotopic variants of the $[M + 43]^-$ formate-like adducts. Some amount of normal formate adducts at $[M + 45]^-$ were formed as normal, but a higher proportion of the population of molecules in the APCI source underwent transformation to the $[M + 43]^-$ formate-like adduct. This made interpretation of (–) APCI-MS spectra, even with chromatographic separation, more complicated. This behavior would make interpretation of (–) APCI-MS spectra obtained by infusion, without prior class separation, highly problematic.

3.7. Negative-ion APCI-MSⁿ mass spectra

Since negative-ion APCI-MS³ mass spectra have not been reported previously for bovine milk sphingomyelin, an example of this data will be given. Fig. 7A shows the location of elution of $d18:1/16:0$ and isobaric species, which gave the formate-like $[M + 43]^-$ adduct at m/z 745.5 in Fig. 6D. The average mass spectrum, Fig. 7B, across the chromatographic peak in Fig. 7A showed the two largest peaks as the $[M + 43]^-$ adduct

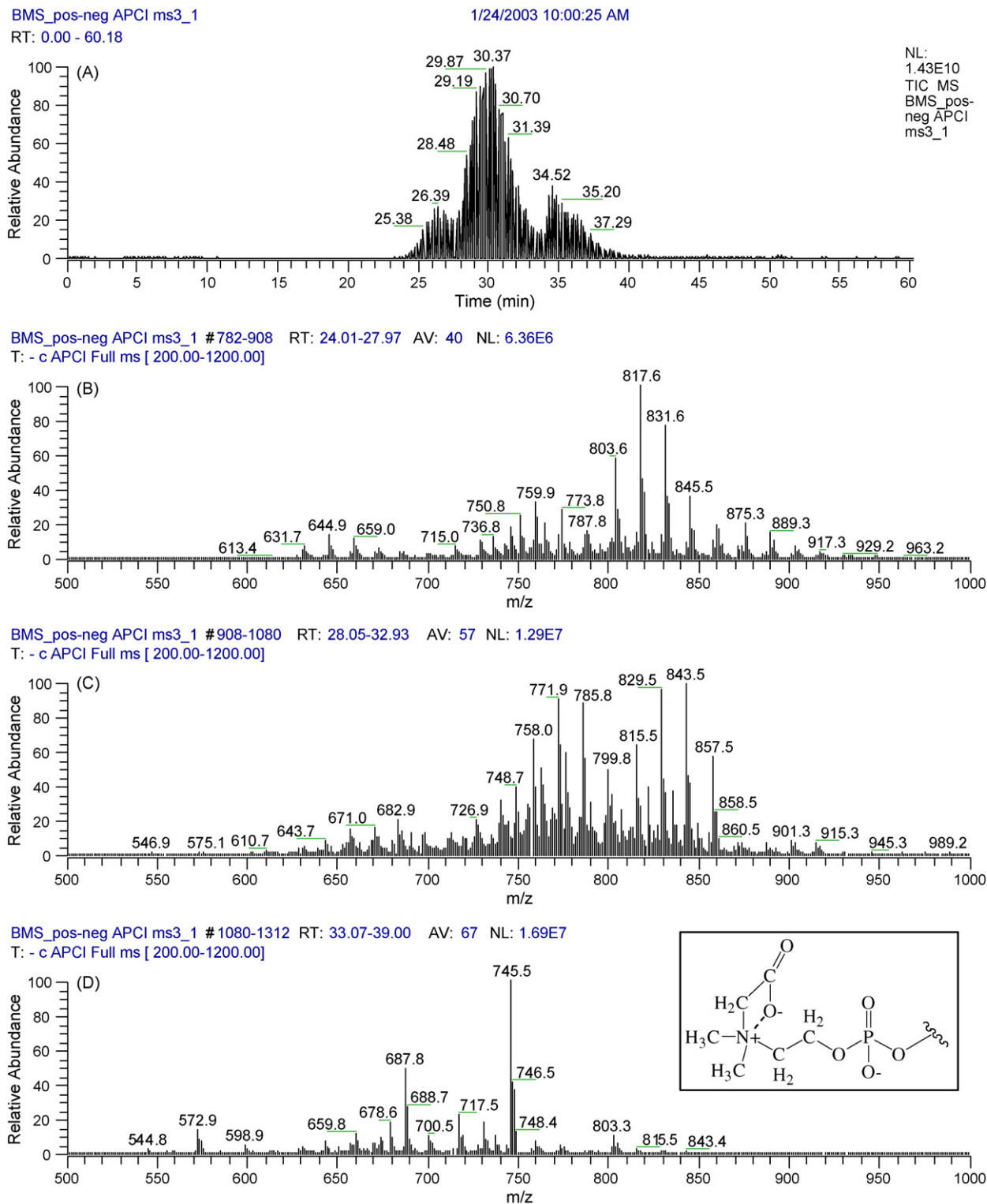


Fig. 6. Negative-ion APCI-MS data for BMS. (A) TIC showing alternating positive and negative APCI-MS scans; (B) average negative-ion mass spectrum across SL1, from 24 to 28 min; (C) average negative-ion mass spectrum across SL2, from 28 to 33 min; (D) average negative-ion mass spectrum across SL3, from 33 to 39 min. Structure of modified formate adduct, $[M + \text{HCOO} - 2\text{H}]^- = [M + 43]^-$ inset. Run not in parallel.

at m/z 745.5 and the $[M - 15]^-$ fragment at m/z 687.8 from *d*18:1/16:0. Since Fig. 7B shows a full-scan mass spectrum, other short-chain SM species also eluted with similar retention times, and gave adducts and fragments in the spectrum. The MS/MS mass spectrum of m/z 745.5, Fig. 7C, exhibited

almost exclusively the $[M - 15]^-$ fragment ion, providing no additional structural information. Most SM and DSM species gave primarily the $[M - 15]^-$ fragment ion in MS/MS spectra. The $(-)$ APCI-MS³ mass spectrum, Fig. 7D, exhibited several ions that could be used to identify the *d*18:1 long-chain

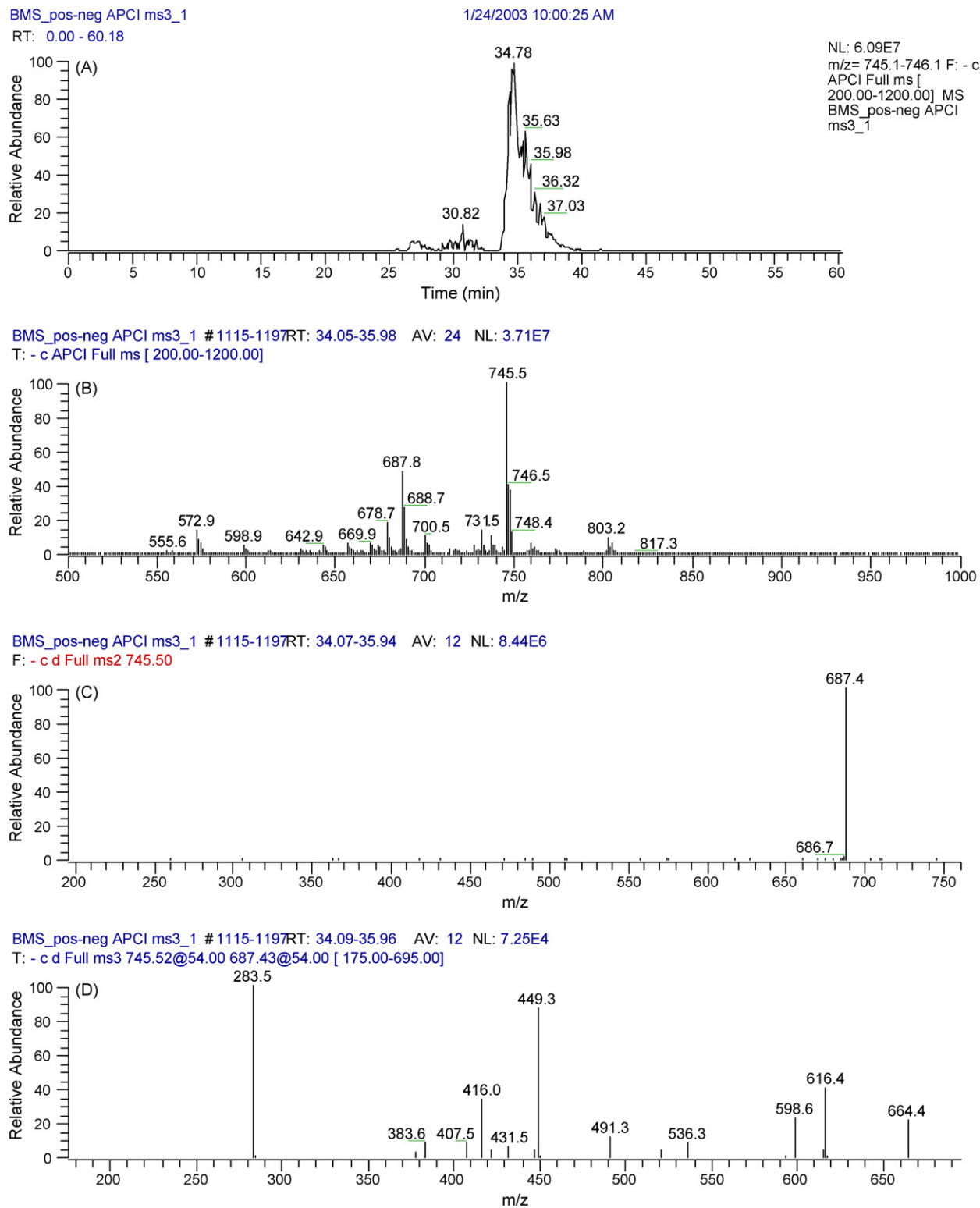


Fig. 7. Negative-ion APCI-MSⁿ data for BMS. (A) EIC of m/z 747.6 in negative-ion mode; (B) average negative-ion mass spectrum from 34 to 36 min; (C) average negative-ion MS/MS mass spectrum of m/z 745.5 precursor, from 34 to 36 min; (D) average negative-ion MS³ mass spectrum of m/z 745.5 \rightarrow m/z 687.4, from 34 to 36 min. Suggested identities of (–)MS³ fragments given in Fig. 8.

base and to specify the intact molecular species, but fragments attributable solely to the FA were not evident. It is possible to suggest likely identities of most of the fragments in the (–) APCI-MS³ mass spectrum in a very straightforward manner by

analogy to structures formed in positive-ion mode reported previously [28]. These are given in Fig. 8. Several fragments, such as those at m/z 616.4 and m/z 598.6 were formed by loss of the *N,N*-dimethylethylamine moiety from the head group, which

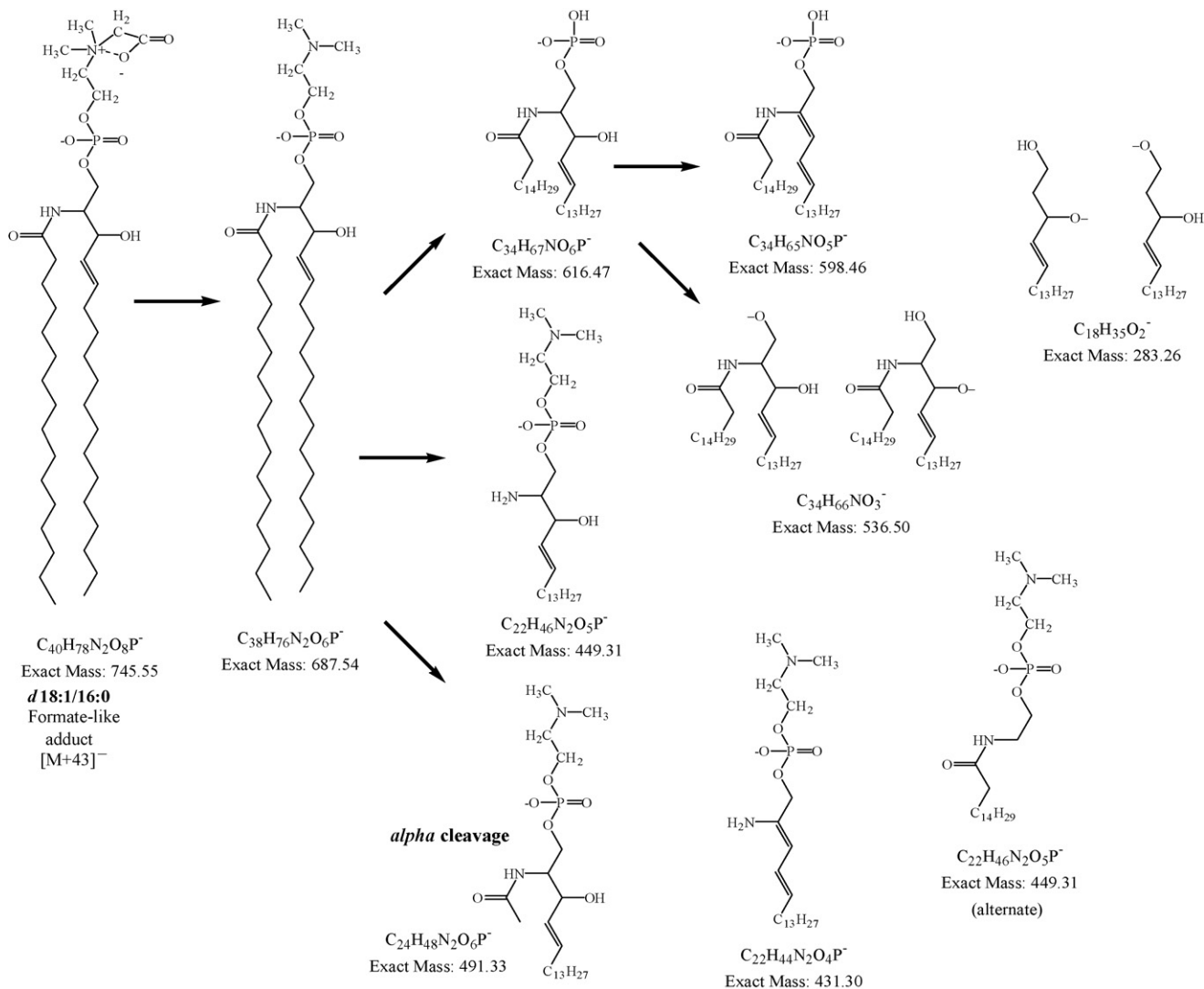


Fig. 8. Suggested fragment identities observed in negative-ion APCI-MS³ mass spectrum (Fig. 7D).

had been formed by loss of a methyl group from the choline, while other fragments, such as *m/z* 491.3, *m/z* 449.3 and *m/z* 431.5 had the *N,N*-dimethylethylamine moiety intact. The *m/z* 283.5 fragment ion allowed the *d*18:1 LCB from *d*18:1/16:0 to be identified, but no other LCB fragments from isobaric species were produced, and no fragments that could be used to directly identify the FA were found. The FA identity was deduced from the larger intact fragments, considered with the *d*18:1 LCB. SM species formed more useful fragments by (−) APCI-MS³ than DSM species did. APCI-MS³ of DSM species in negative-ion mode exhibited fewer fragment ions than SM species, which is in contrast to their behavior in positive-ion mode, as discussed in the preceding report [28]. In fact, very few SM and DSM species gave substantial numbers of fragments in MS³ spectra. These results demonstrated that positive-ion mass spectra were more useful than negative-ion spectra for structural elucidation, since positive-ion spectra produced multiple fragments that specified the identities of several LCBs and FAs that made up the group of isobaric species that were chromatographically overlapped.

3.8. Hydroxy sphingolipids

Morrison and Hay [21] had reported the presence of 2-hydroxy fatty acids in BMS along with normal fatty acids. However, the total combined amount of all species with hydroxy fatty acids was reported to be **less than 1%**. Nevertheless, since it was reported [37] that SL1 was composed of “saturated LCBs with hydroxy-FAs, saturated and/or unsaturated”, it is necessary to discuss hydroxy sphingolipids here. Based on conventional notions of elution on a normal-phase chromatographic system, hydroxy-containing molecular species would be considered more polar and be expected to elute after their non-hydroxy counterparts. Using ESI-MS, we did find evidence for hydroxy-containing SLs present at very low levels that eluted later than their non-hydroxy analogs. For instance, normal *d*18:1/16:0 SM was present as approximately 12.9% of SM species, estimated by APCI-MS in Table 1. The hydroxy-containing variant, *d*18:1/16:0-OH SM has a calculated protonated molecule mass of 719.6 Da (compared to 703.6 Da for normal *d*18:1/16:0 SM). This would give a calculated formate adduct ion, $[M+45]^-$,

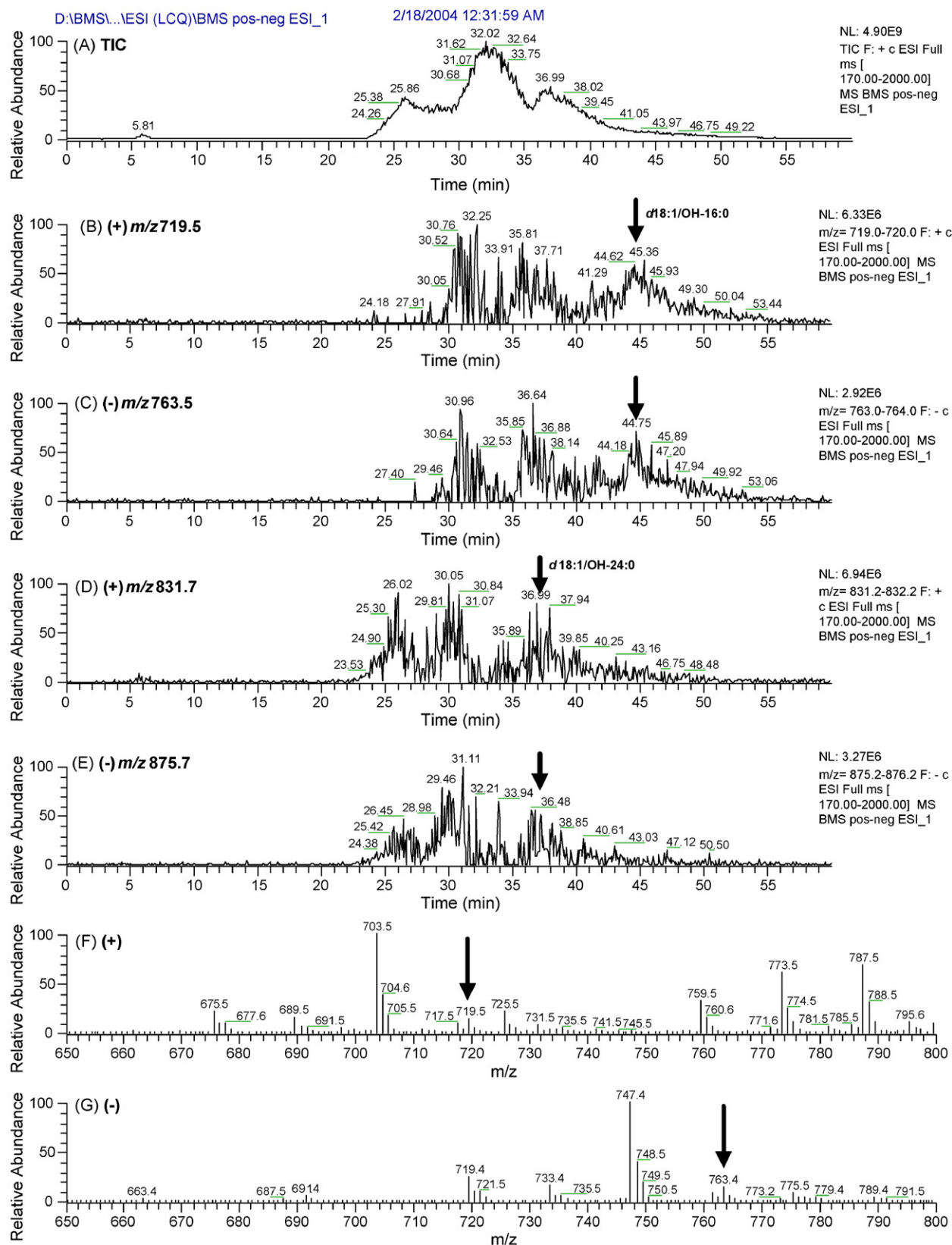


Fig. 9. (A) (+)TIC of BMS by ESI-MS; (B) EIC of the $[M+H]^+$ of $d18:1/OH-16:0$; (C) EIC of the $[M+45]^-$ of $d18:1/OH-16:0$; (D) EIC of the $[M+H]^+$ of $d18:1/OH-24:0$; (E) ESI-MS EIC of the $[M+45]^-$ of $d18:1/OH-24:0$; (F) average (+) mass spectrum from 44 to 47 min; (G) average (-) ESI-MS mass spectrum from 44 to 47 min. Average (-) scans across SL peaks shown in Fig. 5. (+) APCI-MS parallel run not shown.

mass of 763.6 Da by negative-ion ESI-MS. Fig. 9B and C show ion chromatograms of m/z 719.5 (+) and m/z 763.5 (–). The extracted ion chromatograms (EICs) of these two masses showed peaks from 44 to 47 min, which were after the end of SL3. The normal short-chain SM species eluted in SL3, and after these eluted, a small peak likely arising from the hydroxy species was observed, as expected based on chromatographic considerations for the more polar hydroxy-containing molecular species. The normal SM peak at m/z 761.4 in Fig. 9G, shown more clearly in the average spectrum across SL3 in Fig. 5D, represented the isobaric species $d17:1/18:0$, $d18:1/17:0$ and $d19:1/16:0$ in Table 2. These were saturated species, so there were no species in SL3 that had one less site of unsaturation that could give the mass at m/z 763.4 in Fig. 9G. Also, m/z 763.4 was not the $[M+45+2_{\text{isotopic}}]^-$ peak from m/z 761.4, since it was larger than m/z 761.4 peak in the 44 to 47 min retention time range. There were no other SM species that had that mass at that retention time, lending strength to the likelihood that it arose from the $d18:1/16:0\text{-OH}$ SM species proposed.

Nevertheless, the mass spectrum averaged across this small peak was not definitive for the hydroxy species, because we did not obtain multiple mutually confirmatory fragments by APCI-MSⁿ in parallel with the (–) ESI-MS data. There was sufficient carryover from the much larger amounts of normal SLs such that the peaks arising from the hydroxy SLs were small by comparison. The $[M+H]^+$ and $[M+45]^-$ peaks that identified the $d18:1/16:0\text{-OH}$ molecular species are marked with arrows in mass spectra averaged from 44 to 47 min, shown Fig. 9F and G. These peaks were very small in the ESI-MS mass spectra, which were obtained with the ESI source attached to the LCQ ITMS instrument. The data from this run were obtained in parallel with APCI-MS on the TSQ700 instrument. ESI is more sensitive for phospholipid analysis than APCI, and the newer LCQ ITMS instrument is more sensitive than the older TSQ700 instrument, so the hydroxy SM species produced no identifiable signal by APCI-MS on the TSQ instrument. Even with APCI-MS on the ITMS instrument, sufficient abundances of fragments from hydroxy SLs were not observed to allow us to unambiguously identify these species. Nevertheless, ESI-MS on the ITMS machine did allow the presence of the hydroxy SLs at very low levels of to be proposed, as expected from the report of Morrison and Hay [21]. Furthermore, the retention times of the observed low levels of hydroxy sphingolipid species are later than their non-hydroxy analogs, which was consistent with conventional considerations of normal-phase chromatography.

Similarly, the hydroxy-containing variant, $d18:1/24:0\text{-OH}$ SM has a calculated protonated molecule mass of 831.7 Da, compared to 815.7 Da for normal $d18:1/24:0$ SM. This gave a calculated formate adduct ion mass of 875.7 Da in negative-ion ESI-MS mode. Fig. 9D and E show ion chromatograms of m/z 831.7 (+) and m/z 875.7 (–). The EICs of these two masses showed peaks from 36 to 39 min, which is in SL3. The normal long-chain SM species eluted in SL2, and so the hydroxy-containing variants of these species were expected to elute later by NP-HPLC. This would mean that hydroxyl long-chain SM species were expected to elute in SL3, overlapped with the short-chain normal SM species also in SL3. After the normal

$d18:1/24:0$ SM eluted, a small peak arising from the hydroxy species was observed, as expected based on chromatographic considerations for the more polar hydroxy-containing molecular species. The other peaks in the EICs in Fig. 9D and E arose from normal non-hydroxy species eluted in their proper order: long-chain DSM in SL1 and short-chain DSM plus long-chain SM in SL2.

In a previous report [37], SL1 was identified as containing SLs with saturated LCBs with hydroxy-containing long-chain FA. This is counter to commonly accepted concepts of the behavior of molecules separated by normal-phase chromatography, which would indicate that all else being equal, a hydroxy group will cause a molecule to be more polar than its non-hydroxy equivalents and therefore to be retained longer by normal-phase chromatography columns than its non-hydroxy counterparts. The previous report [37] was not in agreement with our previous reports [29,34,38] that showed that SL1 contained normal long-chain dihydrosphingolipids. The initial identification of the long-chain sphingolipid species that eluted in SL1 had been made using both ³¹P NMR and 2D ¹H NMR [38]. We recently presented extensive APCI-MS, MS/MS, MS³ and ESI-MS, MS/MS and MS³ data for bovine brain sphingolipids that confirmed our previous findings [28]. Similarly, the results given in Fig. 3 and elsewhere above conclusively demonstrated the use of $[M+H]^+$, $[\text{Cer-H}_2\text{O}+H]^+$, $[\text{Cer-2H}_2\text{O}+H]^+$, $[\text{LCB}]^+$, $[\text{LCB-H}_2\text{O}]^+$, $[\text{FA}(\text{long})]^+$ and $[\text{FA}(\text{short})]^+$ fragments from dual parallel mass spectrometers for identification of the species eluted in SL1 as being normal long-chain DSM species, in agreement with our previous results.

Morrison [22], Morrison and Hay [21] and Ramstedt et al. [39] have identified the primary fatty acids in bovine milk SLs as being saturated species, with lesser amounts of monounsaturated species. The data in Tables 3 and 4 agree with these previous findings. The masses in Fig. 2B, which are similar to the data in a previous report [37] do not correspond to species that have both a saturated LCB and a hydroxy FA. For instance, if $d18:0/20:0\text{-OH}$ DSM, which is isobaric with $d160:0/22:0\text{-OH}$ DSM and $d170:0/21:0\text{-OH}$ DSM, were present in SL1, any of these species would have a calculated mass of 777.64 Da for the $[M+H]^+$, which is not the major peak in Fig. 2B, or in the previous report [37]. Similarly, if $d18:0/21:0\text{-OH}$ DSM, which is isobaric with $d160:0/23:0\text{-OH}$ DSM and $d170:0/22:0\text{-OH}$ DSM, were present in SL1, these species would have a calculated mass of 791.66 Da for the $[M+H]^+$. Similarly, every sphingolipid that has a saturated long-chain base and a saturated hydroxy fatty amide has a calculated mass 2 Da larger than the peaks in Fig. 2B and in the previous report [37]. Monounsaturated hydroxy fatty amides would give the observed masses, but, as mentioned, it is well known that saturated fatty amides constitute the majority of milk sphingolipid species. Therefore, either all the peaks shown in the mass spectrum averaged across the first sphingolipid peak in the previous report [37] were monounsaturated, which does not agree with the observed FA composition, or the species in SL1 were not hydroxy-containing FA, but were instead normal, non-hydroxy-containing saturated DSM species. Finally, the peaks in the earlier report [37] appear to represent a more substantial proportion of BMS than the 1% of the bovine milk SLs reported

Table 3
Comparison of long-chain base analysis results

Source	12:0	14:0	15:0	16:0	17:0	18:0	19:0	20:0	Sum
Ref. [21] ^a	0.56	0.56	0.56	46.07	8.43	35.39	3.93	4.49	99.99
Ref. [41] ^b	0	0	0	89.92	5.88	4.20	0	0	100.00
APCI ^c	0.25	0.42	0	56.09	5.24	36.47	0.98	0.55	100.00
ESI ^d	0.27	0.39	0	58.39	5.42	34.06	0.91	0.55	99.99

Source	12:1	13:1	14:1	15:1	16:1	17:1	18:1	19:1	20:1	Sum
Ref. [21]	0.61	0.49	1.82	1.34	25.55	10.22	51.58	7.42	0.97	100.00
Ref. [41]	0	0	0	0	33.83	9.23	53.76	3.19	0	100.01
APCI	0	0	0	0	26.03	10.52	60.23	2.98	0.24	100.00
ESI	0	0	0	0	29.59	11.09	57.34	1.86	0.11	99.99

^a Composition of long-chain bases from Ref. [21], determined using GC–FID, with SM and DSM each normalized to 100.00%.

^b Composition of LCBs from Ref. [41], determined using GC/MS, with SM and DSM each normalized to 100.00%.

^c Composition of LCBs from Table 1.

^d Composition of LCBs from Table 2.

Table 4
Comparison of fatty acid composition results

FA	Ref. [21] ^a GC–FID	Ref. [39] ^b GC–MS	Ref. [43] ^c GC–FID	Ref. [42] ^d	APCI ^e	ESI ^f	Avanti ^g
10:0							
12:0	0.1					0.1	
13:0							
14:0	0.4	0.4*	0.4 (.02)	1.0	1.0	2.0	
14:1					0.1	0.1	
15:0	0.1	0.4*	0.1 (.00)		0.2	0.4	
15:1					0.1	0.1	
16:0	7.8	13.5	7.4 (.14)	49.0	16.5	29.9	19
16:1					0.2	0.6	
17:0	0.3	0.8	0.2 (.00)		0.5	0.6	
17:1					0.1	0.1	
18:0	1.6	2.5	2.8 (.06)	1.0	1.5	2.3	3
18:1	0.2	0.8*	1.9 (.02)		0.2	0.3	
18:2	0.2						
19:0	0.2				0.1	0.1	
20:0	0.6	1.0	0.8 (.01)		0.4	0.6	1
20:1				3.0	0.6	0.2	
21:0	0.9	1.8	0.6 (.01)		0.7	0.8	
21:1					0.8	0.7	
22:0	20.7	22.1	21.8 (.06)	18.0	15.8	16.3	19
22:1	0.7				1.0	0.6	
23:0	30.4	31.4	24.4 (0.9)	20.0	29.8	23.7	33
23:1	5.0		3.4 (.15)		3.6	2.8	
24:0	22.8	19.1	24.8 (.15)	8.0	20.2	13.8	20
24:1	4.0	4.8	4.5 (.22)		3.5	2.3	3
25:0	1.6	1.0	0.9 (.07)		1.0	0.6	
25:1	1.6	0.4*	1.3 (.06)		1.2	0.8	
26:0	0.8		0.9 (.05)		0.7	0.4	
26:1			0.2 (.02)		0.3	0.1	
Other			3.8				2(20:4)
	100.0	100.0	100.2	100.0	100.1	100.3	100.0

^a Results from GC–FID analysis of buttermilk powder extract, Ref. [21].

^b Results for Avanti Polar Lipids BMS approximated by manually measuring graphs in Ref. [39] (values were not given). Values marked with asterisks had a high degree of uncertainty.

^c Results from GC–FID analysis of BMS from Karlshamns LipidTeknik, Ref. [43] with (SD).

^d Results from GC–FID analysis of BMS by SMR, Swedish Dairies' Association, Ref. [42].

^e Net FA composition determined from species given in Table 1, by APCI-MS.

^f Net FA composition determined from species given in Table 2, by ESI-MS.

^g Composition for BMS FA given on Avanti Polar Lipids website.

by Morrison and Hay [21]. Since the all hydroxy-SL species combined represented less than 1% of the composition, the individual molecular species were present at very low levels. The hydroxy-SLs were present at levels below which their quantities could be estimated using the multiple mutually confirmatory fragments employed by us.

3.9. Comparison to previous reports

In 1994, Valeur et al. [40] reported the use of HPLC/thermospray ionization mass spectrometry for analysis of bovine milk and other sphingomyelin species. They used reversed-phase (RP) HPLC for separation of the SLs, so the SLs were not separated by class, but were instead separated by carbon chain length and degree of unsaturation. Only SM species, with no DSM species, were identified.

In 1998, Karlsson et al. [37] reported the use of HPLC/atmospheric pressure chemical ionization (APCI) MS and HPLC/electrospray ionization (ESI) MS for analysis of bovine milk sphingomyelin and other commercially available sphingolipids. APCI-MS/MS was used to obtain structural information to identify the long-chain base and fatty amide portions of the molecules. An ‘up-front’ collision-induced dissociation (CID) voltage of 30 V was used. The authors employed a diol column to perform the normal-phase separation of sphingolipid species, and showed elution of three sphingolipid peaks for bovine milk, which were identified as: SM1, saturated long-chain base with hydroxy fatty acids (saturated and unsaturated); SM2, unsaturated LCB with long-chain fatty acids (saturated and unsaturated); and SM3, unsaturated LCB with short chain fatty acids (saturated and unsaturated). A saturated long-chain base is a dihydroceramide backbone, so a saturated long-chain base with a hydroxy fatty acid would be a DSM species with a hydroxy fatty acid. The authors used an asterisk ranking system to provide an indication of the relative amounts of species. In bovine milk, the tabulated results showed 23 SM species and 5 DSM species, as well as 5 hydroxy-FA SM species. No DSM species having hydroxy-FA were tabulated.

In the previous report of APCI-MS of BMS [37], MS/MS mass spectra of m/z 606 across SL1 and SL2 were shown. The spectrum across SL2 (Ref. [37], Fig. 7 lower panel) showed a peak at m/z 238.0 that was labeled ‘LCB 16:0-H₂O’ and a peak at m/z 255.4 that was labeled ‘LCB 16:0’, identifying the molecular species as a 16:0 DSM. The fragment at m/z 392.1 was labeled ‘FA 24:0’. The LCB fragment taken with the FA fragment indicated a $d16:0/24:0$ DSM molecular species. However, we showed with substantial evidence above and in our previous reports that DSM species containing long-chain FA eluted in SL1, not SL2. The peak at m/z 789 in SL2 that gave the fragment at m/z 606 in the previous report [37] did not correspond to a DSM species, but instead likely corresponded to the $2 \times ^{13}\text{C}$ or $1 \times ^{13}\text{C} + 1 \times ^2\text{H}$ isotopic variant of $d16:1/24:0$ SM. This was evidenced by the [LCB]⁺ fragment in Fig. 7 in that report, which occurred at m/z 255.4 instead of at its monoisotopic mass of m/z 254.3. That fragment contained either a ¹³C or a ²H that caused it to appear at 1 m/z higher than its correct monoisotopic mass. In our preceding report [28], Fig. 2 showed EICs of both m/z 604.6

and m/z 606.6 to demonstrate that the m/z 604.6 EIC had its major peak in SL2 at the same time where the minor peak in the EIC of m/z 606.6 occurred. This was used to demonstrate that the [Cer-H₂O + H]⁺ fragment of $d18:1/22:0$ at m/z 604.6 produced a [Cer-H₂O + H + 2_{isotopic}]⁺ variant at m/z 606.6 that was observed at the same retention time. According to the program ‘Molecular Weight Calculator v. 6.22’, the +2 isotopic variant would have a calculated abundance at m/z 606.7 that is 13.98% of the abundance of the monoisotopic mass at m/z 604.7.

The peak at m/z 789 in SL1 in Ref. [37] that gave the fragment at m/z 606 exhibited an MS/MS spectrum that showed fragments at m/z 365.4 and m/z 393.4, which were identified as ‘FA OH-21:0’ and ‘FA OH-23:0’. However, these odd-mass fragments did not obey the nitrogen rule applicable to protonated fragments from the fatty amide chains. The m/z values were not at the proper monoisotopic masses for the proposed species, which were 366.3 m/z and 394.4 m/z respectively. Furthermore, as mentioned above, hydroxy-containing species are not expected to elute before their non-hydroxy counterparts by NP-HPLC.

Semi-quantitative results were given in Tables 1 and 2. The long-chain base compositions determined by APCI-MS and ESI-MS were compared to those determined by Morrison and Hay [21], Morrison [22] and by Olsson et al. [41]. As mentioned above, Morrison and Hay used a complex extraction, separation and derivatization process involving extraction, silica column chromatography, refluxing, silica column chromatography again, treatment with *phospholipase C* to yield ceramide, crystallization, thin-layer chromatography (TLC), base hydrolysis, extraction, preparation of dinitrophenyl derivatives, separation by TLC, extraction, oxidation to aldehydes with periodate, and finally GC analysis of the aldehydes, which was confirmed with GC/MS. They identified *iso* (n-1) and *anteiso* (n-2) branched-chain LCBs in buttermilk powder (18.5% of LCBs) as well as normal LCBs. The branched chain fatty acids were not differentiated using our APCI-MS and ESI-MS approach, so all normal and branched C_x:U_y (carbon number:unsaturation) species reported by others were grouped together in Table 3 for comparison to our results.

Olsson et al. [41] used a derivatization process that involved *sphingomyelinase* hydrolysis to ceramide, extraction, acidic hydrolysis to free LCBs, extraction, reaction with acetic anhydride to form the *N*-acetates, and reaction with *N*-(trimethylsilyl)-imidazole to produce TMS derivatives, followed by GC/MS analysis. Since they used GC for separation of the LCB derivatives, they also separated *iso* and *anteiso* branched LCB structures (26.6% of LCBs, unnormalized), which are grouped with normal LCBs by C_x:U_y in Table 3. The BMS SL sample used in that report was prepared at Scotia LipidTeknik (Stockholm, Sweden).

The number of DSM long-chain bases identified in BMS by us was similar to the number of species identified in buttermilk powder by Morrison. We identified DSM LCB species from 12:0 to 20:0, excluding 15:0. Since we were aware of the previous work [21] we looked closely for species having the 15:0 LCB, but could not produce definitive evidence, based on multiple mutually confirmatory fragments, of their presence. However,

as Tables 1 and 2 show, only low levels of few species containing the 12:0 and 14:0 LCBs were seen, so it could be the case that our instrument was not able to detect the low levels of 15:0 LCB-containing species. We have shown that the instrument used here is more sensitive and identified more species than were reported in our earlier reports [29,34] using older instruments. As LC/MS technology continues to improve, it is likely that newer generations of more sensitive LC/MS instruments will allow identification of additional intact molecular species at low levels having other FAs in combination with these LCBs. At the current level of technology some LCB/FA combinations probably remain below our current limit of detection. Nevertheless, we have identified more intact species by online LC/MS than have been identified in the past.

The amounts of several monounsaturated SM LCB species reported by us in BMS are remarkably similar to the amounts reported in buttermilk powder by Morrison and Hay [21]. However, we did not find any species containing the *d*12:1, *d*13:1, *d*14:1 or *d*15:1. Likewise, Olsson et al. [41] did not report any of these species. Although it would be convenient to assume that the results by Olsson et al. confirm our results that these species were not present, other results by Olsson et al. seem to indicate that perhaps some species were not observed using the GC/MS approach because the mass spectra obtained in electron ionization (EI) mode were much more complex and the species were not well resolved chromatographically, so small amounts of overlapped species could not be easily recognized. The fact that *d*12:0, *d*14:0, *d*15:0, *d*19:0 and *d*20:0 LCBs were also not identified in that report [41], although we did identify these species based on multiple fragments, indicates that the complex nature of EI-MS spectra may cause problems for LCB analysis. Since there are so few results to compare, a consensus cannot yet be achieved regarding the number of SM LCBs present in BMS. We will not be surprised if newer generations of LC/MS instruments are able to identify low levels of SM LCBs that are not currently evident. We also do not know the effect that different milk extraction and SL sample preparation techniques had on the reported SL compositions. Nevertheless, we have identified all of the primary LCBs intact using online LC-MS, without the need for derivatization.

When comparing results by GC-FID, GC-MS and LC-MS, the dramatic advantage of our approach is that intact individual molecular species can be seen, instead of just the net LCB composition found by decomposing all SL species. This allows differences between LCB/FA associations to be identified. For instance, Tables 1 and 2 show that the LCB *d*16:0 has a preference for association with long-chain FA such as 22:0, 23:0 and 24:0 over short-chain FA, whereas *d*18:0 is found with similar levels of *d*18:0/23:0 and *d*18:0/16:0. This type of information showing potential preferences for individual combinations of molecular species is lost when all LCBs are hydrolyzed and derivatized for GC analysis.

From Tables 1 and 2 we were able to calculate a net FA composition based on all SL molecular species. This is given in Table 4, along with literature results. Our results by APCI-MS are very similar to those by Morrison and Hay [21], except that we reported a higher percentage of the 16:0 fatty acid and

a lower level of 22:0. Other molecular species were surprisingly similar, given the different samples, sample preparation, and very different analysis techniques. We were able to identify a larger variety of monounsaturated FA species than those reported elsewhere [21]. For example, the *m/z* 773.5 [M+H]⁺ ion, which is clearly visible in Fig. 2B, arose from a saturated LCB combined with a monounsaturated FA, and so eluted in SL1. Although several isobaric species were possible, Table 2 showed that this species was *d*18:0/21:1 (instead of *d*16:0/23:1, *d*17:0/22:1, *d*19:0/20:1 or *d*20:0/19:1), based on confirmation by [LCB]⁺, [LCB-H₂O]⁺, [FA(short)]⁺ and [FA(long)]⁺ fragments. Similarly, the *m/z* 771.4 peak, clearly visible in Fig. 2C was identified as arising from *d*18:1/21:1. Corresponding [M+45]⁻ peaks at *m/z* 817.5 and *m/z* 815.6 in the negative-ion spectra in Fig. 5B and C, respectively, further confirmed the identifications made based on positive-ion ESI-MS and APCI-MSⁿ spectra. Thus, several mutually confirmatory pieces of data were used to identify the presence of monounsaturated molecular species, such as that containing the 21:1 fatty amide chain, that were not reported by other authors.

Results by Ramstedt are shown, but these were obtained from the apparent FA composition manually measured in a magnified version of the graph presented in Ref. [39], since values for the FA composition were not given. Because of the high degree of uncertainty associated with such an approximation, those results are not further discussed. Results by Nyberg [42] are listed, but these show substantial differences to all other results, such as the large amount of 16:0, and a larger amount of 20:1 than 18:0, 20:0 or 21:0, and so are not further discussed.

The results by Olsson et al. [43], obtained by GC-FID are similar in most respects to those of Morrison and Hay [21], although a smaller proportion of 23:0 was identified. Our results determined by APCI-MS also agree fairly well with those results, except that we report a larger amount of 16:0 (16.5% by APCI-MS). The results given by the supplier of the BMS, Avanti Polar Lipids, also indicate a larger amount of 16:0, reported to be 19%. However, the results by the supplier do not describe any monounsaturated species, which are clearly present based on the results given here and previously [21,43]. They also listed 20:4 as being present at a level of 2%, which was not confirmed by our results or any literature reports, so that FA composition cannot be taken as complete and accurate.

If the composition provided by the supplier is used simply as an approximation of the primary saturated species, it can be used to point to a potential trend in the ESI-MS data compared to the APCI-MS data. It appears that the ESI-MS data resulted in a larger calculated composition of short-chain species and a smaller percentage of long-chain FA. This is evident by comparison of the ESI-MS data to both the APCI-MS data and the supplier's data. The APCI-MS data provides better agreement to the manufacturer's composition for the primary saturated species. All of our data and the supplier's data indicate that there was a larger proportion of the 16:0 FA in BMS from this source than was reported for the samples analyzed by most others.

The data in Table 4 illustrate several points: (1) there are likely compositional differences between BMS samples that have been extracted, prepared and analyzed by different tech-

niques; (2) there is not yet a consensus on the composition of FAs in BMS; and (3) there is a need for high quality GC–MS data to identify FAs in SL samples that are now widely commercially available. Literature suggests that it may be difficult to identify FAs present at low levels using GC–EI/MS. There is a need for updated GC/MS data obtained on modern sensitive instruments using softer ionization methods such as chemical ionization. Over a decade ago, APCI–MS was combined with SFC [44] for analysis of FA methyl esters and other molecules, but it has not yet been applied to FAs from SLs. More recently, articles are starting to appear that employ APCI–MS as a detector for GC [45]. As the interest in SLs grows, due to their involvement in many biological processes, it will become even more important to have updated analytical techniques available for their analysis. In the meantime, we have shown that online APCI–MS and ESI–MS coupled to NP–HPLC are capable of determining the composition of numerous intact molecular species, and from the composition of intact species the composition of FA can be determined. We have provided data that clearly showed that monounsaturated FA were present that have not been identified using other techniques.

4. Conclusion

We have described herein the analysis of sphingolipids first by employing a normal-phase chromatographic system to separate the classes of DSM and SM, followed by detection using two complementary API–MS techniques, APCI–MS and ESI–MS, obtained simultaneously in parallel. The information derived from mass spectra may be summarized as follows:

- The APCI–MS technique produced primarily $[\text{Cer-H}_2\text{O} + \text{H}]^+$ and $[\text{Cer-2H}_2\text{O} + \text{H}]^+$ fragment ions, while the ESI–MS technique produced protonated molecules from each molecular species. The $[\text{M} + \text{H}]^+$ ions allowed confirmation of the molecular weight of any species identified based on the $[\text{Cer-H}_2\text{O} + \text{H}]^+$ and $[\text{Cer-2H}_2\text{O} + \text{H}]^+$ fragments. Separate runs were performed to obtain APCI–MS/MS and MS^3 data.
- APCI–MS/MS of the $[\text{Cer-H}_2\text{O} + \text{H}]^+$ ion precursor gave long-chain base fragments, $[\text{LCB}]^+$ and $[\text{LCB-H}_2\text{O}]^+$, that allowed the class of sphingolipid to be determined as either a sphingomyelin or a dihydrosphingomyelin, and allowed the length of the LCB to be determined.
- APCI–MS/MS and MS^3 of the $[\text{Cer-H}_2\text{O} + \text{H}]^+$ and $[\text{Cer-2H}_2\text{O} + \text{H}]^+$ ions produced fatty amide fragments, $[\text{FA}(\text{long})]^+$ and $[\text{FA}(\text{short})]^+$, that allowed the identities of the fatty amide chains to be identified in terms of the length of the FA chain and the degree of unsaturation.

The results obtained in positive-ion mode were confirmed by ESI–MS, APCI–MS and APCI–MSⁿ in negative ion mode. We identified a formate-like adduct, $[\text{M} + 43]^-$, for the first time in negative-ion APCI–MS mass spectra, and contrasted it to the normal formate adduct, $[\text{M} + 45]^-$, formed by negative-ion ESI–MS. We showed for the first time that the formate-like adduct in (–) APCI–MS could be used as a precursor to yield APCI–MS/MS and MS^3 negative-ion mass spectra that allowed direct

identification of the LCB, as well as fragments containing the LCB/FA combination that allowed the identity of the FA to be determined.

We have used multiple positive- and negative-ion ESI–MS and APCI–MS techniques to conclusively show that normal-phase HPLC for separation of SLs produced three primary peaks consisting of: SL1, long-chain FAs combined with saturated LCBs to give long-chain DSM species; SL2, short-chain FAs combined with saturated LCBs to give short-chain DSM species, which were chromatographically overlapped with long-chain FAs attached to monounsaturated LCBs, to give long-chain SM species; and SL3, short-chain FAs attached to monounsaturated LCBs, to give short-chain SM species. These findings were in agreement with our previous reports.

³¹P NMR spectroscopy data were provided to further demonstrate that substantial levels of DSM species are present in BMS. Combined with the mass spectrometry data, the ³¹P NMR spectroscopy data were conclusive for the presence of DSM species. Our results showed more molecular species than have previously been reported by LC/MS. We have conclusively identified numerous dihydrosphingomyelin species that were not identified using other LC/MS techniques.

The results above, combined with previous reports that identified DSM species by derivatization, indicate that bovine milk contains more dihydrosphingomyelin species than bovine brain. The substantial presence of DSM in bovine milk means that it represents a dietary sphingolipid, which constitutes 15 to 20% of the SLs in bovine milk. This has important implications, based on recent developments in the understanding of the role of SLs in cellular signaling pathways.

We have shown that APCI–MS data of sphingolipids can be complex, and require careful interpretation using supplemental MS/MS data. Also, the very simple ESI–MS data are invaluable to provide confirmation of species identified by APCI–MS. Since APCI–MS produces some in-source fragmentation, some cases of isobaric fragments were observed. APCI–MS/MS data and ESI–MS data were valuable for eliminating any ambiguity, and for apportioning peaks arising from isobaric molecular species. Because of the fragments that are already produced in the APCI–MS source, additional fragmentation by application of an ‘up-front CID’ voltage between the capillary outlet and the skimmer or between the skimmer and the first multipole ion focusing element should be avoided. The non-specific fragmentation caused by ‘up-front CID’ can complicate spectra and lead to misinterpretation. Instead, APCI–MS/MS should be performed so that knowledge of the specific precursor → product, relationship can be maintained. We have also demonstrated that protonated molecules and fragments containing $2 \times {}^{13}\text{C}$ or $1 \times {}^{13}\text{C} + 1 \times {}^2\text{H}$ isotopic variants should be expected and properly recognized for proper identification of SL molecular species. Since DSM species differ from SM species by only 2 Da, the chromatographic resolution of DSM from SM species is crucial to proper identification of all species. The isotopic variants of DSM are isobaric with normal SM, so chromatographic resolution is important to distinguish the isotopic variants.

We have also demonstrated that ³¹P NMR spectroscopy is a very valuable tool for confirming the presence of DSM and SM,

and may be more useful than mass spectrometry for quantification without response factors.

References

- [1] Y. Hannun, R.M. Bell, *Science* 243 (1989) 500.
- [2] Y.A. Hannun, R.M. Bell, *Adv. Lipid Res.* 25 (1993) 27.
- [3] Y.A. Hannun, *J. Biol. Chem.* 269 (1994) 3125.
- [4] S. Spiegel, A.H. Merrill, *FASEB J.* 10 (1996) 1388.
- [5] R. Testi, *Trends Biochem. Sci.* 21 (1996) 468.
- [6] H. Vesper, E.M. Schmelz, M.N. Nikolova-Karakashian, D.L. Dillehay, D.V. Lynch, A.H. Merrill, *J. Nutr.* 129 (1999) 1239.
- [7] P.S. Sastry, K.S. Rao, *J. Neurochem.* 74 (2000) 1.
- [8] J. Raulin, *Lipids* 35 (2000) 123.
- [9] V.A. Struchkov, N.B. Strazhevskaya, *Biochemistry (Mosc)* 65 (2000) 525.
- [10] A.E. Cremesti, A.S. Fischl, *Lipids* 35 (2000) 937.
- [11] G.M. Jenkins, *Cell Mol. Life Sci.* 60 (2003) 701.
- [12] U.P. Steinbrecher, A. Gomez-Munoz, V. Duronio, *Curr. Opin. Lipidol.* 15 (2004) 531.
- [13] S.A. Summers, D.H. Nelson, *Diabetes* 54 (2005) 591.
- [14] A. Bielawska, H.M. Crane, D. Liotta, L.M. Obeid, Y.A. Hannun, *J. Biol. Chem.* 268 (1993) 26226.
- [15] L.M. Obeid, C.M. Linardic, L.A. Karolak, Y.A. Hannun, *Science* 259 (1993) 1769.
- [16] W.D. Jarvis, F.A. Fornari, R.S. Traylor, H.A. Martin, L.B. Kramer, R.K. Erukulla, R. Bittman, S. Grant, *J. Biol. Chem.* 271 (1996) 8275.
- [17] P.J. Hartfield, G.C. Mayne, A.W. Murray, *FEBS Lett.* 401 (1997) 148.
- [18] E.V. Dyatlovskaya, *Russ. J. Bioorg. Chem.* 28 (2002) 5.
- [19] M. Kuikka, B. Ramstedt, H. Ohvo-Rekila, J. Tuuf, J.P. Slotte, *Biophys. J.* 80 (2001) 2327.
- [20] O. Hwang, G. Kim, Y.J. Jang, S.W. Kim, G. Choi, H.J. Choi, S.Y. Jeon, D.G. Lee, J.D. Lee, *Mol. Pharm.* 59 (2001) 1249.
- [21] W.R. Morrison, J.D. Hay, *Biochim. Biophys. Acta* 202 (1970) 460.
- [22] W.R. Morrison, *Biochim. Biophys. Acta* 176 (1969) 537.
- [23] R.C. Gaver, C.C. Sweeley, *J. Am. Oil Chem. Soc.* 42 (1965) 294.
- [24] B. Samuelsson, K. Samuelsson, *J. Lipid Res.* 10 (1969) 47.
- [25] B. Samuelsson, K. Samuelsson, *J. Lipid Res.* 10 (1969) 41.
- [26] R.G. Jensen, *J. Dairy Sci.* 85 (2002) 295.
- [27] J. Adams, *Q. Ann. Mass Spectrom. Rev.* 12 (1993) 51.
- [28] W.C. Byrdwell, R.H. Perry, *J. Chromatogr. A* 1133 (2006) 149.
- [29] W.C. Byrdwell, *Rapid Commun. Mass Spectrom.* 12 (1998) 256.
- [30] B.J. Pettus, A. Bielawska, B.J. Kroesen, P.D.R. Moeller, Z.M. Szulc, Y.A. Hannun, M. Busman, *Rapid Commun. Mass Spectrom.* 17 (2003) 1202.
- [31] W.C. Byrdwell, W.E. Neff, *Rapid Commun. Mass Spectrom.* 16 (2002) 300.
- [32] P. Meneses, T. Glonek, *J. Lipid Res.* 29 (1988) 679.
- [33] J.L. Kerwin, A.R. Tuininga, L.H. Ericsson, *J. Lipid Res.* 35 (1994) 1102.
- [34] W.C. Byrdwell, D. Borchman, *Ophthalmic Res.* 29 (1997) 191.
- [35] X. Han, R.W. Gross, *J. Am. Soc. Mass Spectrom.* 6 (1995) 1202.
- [36] S. Uran, A. Larsen, P.B. Jacobsen, T. Skotland, *J. Chromatogr. B* 758 (2001) 265.
- [37] A.A. Karlsson, P. Michelson, G. Odham, *J. Mass Spectrom.* 33 (1998) 1192.
- [38] W.C. Byrdwell, D. Borchman, K.G. Porter, M.C. Yappert, *Invest. Ophthalmol. Vis. Sci.* 35 (1994) 4333.
- [39] B. Ramstedt, P. Leppimaki, M. Axberg, J.P. Slotte, *Eur. J. Biochem.* 266 (1999) 997.
- [40] A. Valeur, N.U. Olsson, P. Kaufmann, S. Wada, C.G. Kroon, G. Westerdahl, G. Odham, *Biol. Mass Spectrom.* 23 (1994) 313.
- [41] N.U. Olsson, P. Kaufmann, S. Dzeletovic, *J. Chromatogr. B* 698 (1997) 1.
- [42] L. Nyberg, in: G. Cevc, F. Paltauf (Eds.), *Phospholipids: Characterization, Metabolism, and Novel Biological Applications*, AOCS Press, Champaign, IL, 1995.
- [43] N.U. Olsson, P. Kaufmann, C.G. Kroon, *Chromatographia* 34 (1992) 529.
- [44] L.N. Tyrefors, R.X. Moulder, K.E. Markides, *Anal. Chem.* 65 (1993) 2835.
- [45] P. Ostman, L. Luosujarvi, M. Haapala, K. Grigoras, R.A. Ketola, T. Kotiaho, S. Franssila, R. Kostiainen, *Anal. Chem.* 78 (2006) 3027.